

# Fast Hypergraph Regularized Nonnegative Tensor Ring Factorization Based on Low-Rank Approximation

Xinhai Zhao<sup>a</sup>, Yuyuan Yu<sup>a</sup>, Guoxu Zhou<sup>a,\*\*</sup>, Qibin Zhao<sup>a,b,\*\*</sup>, Weijun Sun<sup>a,c</sup>

<sup>a</sup>*School of Automation, Guangdong University of Technology, Guangzhou, China*

<sup>b</sup>*The Center for Advanced Intelligence Project (AIP), RIKEN, Tokyo, Japan*

<sup>c</sup>*Guangdong Key Laboratory of IoT Information Technology, Guangzhou, China*

---

## Abstract

For the high dimensional data representation, nonnegative tensor ring (NTR) decomposition equipped with manifold learning has become a promising model to exploit the multi-dimensional structure and extract the feature from tensor data. However, the existing methods such as graph regularized tensor ring decomposition (GNTR) only models the pair-wise similarities of objects. For tensor data with complex manifold structure, the graph can not exactly construct similarity relationships. In this paper, in order to effectively utilize the higher-dimensional and complicated similarities among objects, we introduce hypergraph to the framework of NTR to further enhance the feature extraction, upon which a hypergraph regularized nonnegative tensor ring decomposition (HGNTNTR) method is developed. To reduce the computational complexity and suppress the noise, we apply the low-rank approximation trick to accelerate HGNTNTR (called LraHGNTNTR). Our experimental results show that compared with other state-of-the-art algorithms, the proposed HGNTNTR and LraHGNTNTR can achieve higher performance in clustering tasks, in addition, LraHGNTNTR can greatly reduce running time without decreasing accuracy.

*Keywords:* Clustering, Low-rank approximation, Hypergraph, Tensor ring decomposition

---

## 1. Introduction

Nowadays, extracting meaningful features from high-dimensional data has always been an important topic in pattern recognition and machine learning. Nonnegative matrix factorization (NMF) has been received plenty of attention [1]. However, with the development of data mining or acquisition and multi-sensor technology, more and more high-dimensional and large data are generated. They also emphasize that the limitation of the flat-view matrix models [2]. Tensors are the multi-dimensional extension of matrices, which can preserve the structural information of high-order data. In recent years, tensor ring decomposition (TR) has been proposed and demonstrated great potentials in image completion and clustering [3, 4]. The tensor ring decomposition essentially expresses the information of each dimension in tensors in the form of a three-order core tensor. Moreover, the TR complexity is increasing linearly with the dimension increasing and it can alleviate the curse of dimension. In other words, TR is

---

\*Corresponding author

\*\*Corresponding author

*Email addresses:* `gx.zhou@gdut.edu.cn` (Guoxu Zhou), `qibin.zhao@riken.jp` (Qibin Zhao)

highly suitable for higher-order tensor analysis. To learn the localized parts of tensor objects, Yu *et al.* proposed the non-negative tensor ring decomposition (NTR) [5].

Nonnegative tensor models have the abilities to discover local-parts based information and take full advantages of the multi-linear structure of data. Many researchers recently have found that data can be thought of as a low-dimensional non-linear manifold embedded in high-dimensional data space [6, 7]. Because manifold learning can learn the intrinsic manifold structure of data, nonnegative tensor decomposition methods that combine with manifold learning showed better performance in many tasks and hence gained great popularity in recent years. Cai *et al.* explored the geometrical information by constructing the nearest neighbours graph and proposed the graph regularized nonnegative matrix factorization (GNMF) [8]. However, the GNMF can only perform feature extraction from vector data. Yu *et al.* proposed the graph regularized non-negative tensor ring decomposition (GNTR) to learn the localized parts of tensor objects and capture the manifold information[5]. But the learned graph from GNTR only models the pairs of similarity relationships between two objects and the manifold information of data can not be sufficiently learned especially in the high-dimension.

There are two main problems in the above-mentioned methods: (1) they do not take the character of higher-order manifold similarity relations of tensor data into consideration, for example, in graphs, we can easily obtain the similarity relations between two samples, but we can not predict if there exist more than two samples having similarity. Therefore, the operation that complex relationships among objects are simply squeezed as pair-wise forms inevitably results in manifold information loss. (2) most of the manifold methods adopt the Gaussian kernel to measure the distance between two samples. It has been proved that the normal two-order graph may be easily affected by the radius parameter  $\sigma$  of the Gaussian kernel [9]. These two major issues can largely be overcome by using hypergraph. The hypergraph is not limited to learning only one connection relationship of both data samples, but also the multi-level connection relationship among the multiple data samples [10]. A graph is a special case of hypergraph with each edge containing two vertices [11]. Zeng *et al.* incorporated the manifold regularized hypergraph with the standard NMF framework. They proposed the hypergraph regularized nonnegative matrix factorization (HNMF) [12]. But it is also limited in its ability to discover the multi-linear structure of data. Yin *et al.* pointed that contrasting the normal graph method, the hypergraph has the better ability to extract the local and high-order geometry structure information. So they combined the nonnegative Canonical Polyadic (CP) decomposition with hypergraph and proposed the HyperNTF [13]. However, this model is difficult to be optimized. And it also has a slow convergence rate.

When large volumes of high-dimensional data become increasingly common, it is time-consuming obviously to analyze these data due to their high storage requirements and high computational complexity. Fortunately, the meaningful features usually also have relatively low-rank properties [14, 15]. A much smaller number of potential variables and components can contain most of the meaningful features of data. Therefore, low-rank approximation methods can be used to preprocess the obtained data. Zhou *et al.* aiming at the problems of slow convergence and excessive computational complexity, they introduced the low-rank approximation to NMF and nonnegative Tucker decomposition (NTD) [16, 17].

In this paper, we propose a novel non-negative tensor ring decomposition method to learn the local-parted features and capture the high-dimensional manifold structure information simultaneously. The combination can learn the manifold information completely and is significantly beneficial to improve the clustering performance. This proposed method is called hypergraph regularized non-negative tensor ring decomposition (HGNTR). Considering that the computation of HGNTR has a large complexity, we introduce the method of low-rank approximations into the HGNTR, then propose the LraHGNTR to reduce running time and suppress noise. The main contributions of this article include the following aspects:

- (1) HGNTR integrates the novel method of hypergraph with nonnegative tensor ring decomposition, can effectively learn the local-parted attributes of tensor data, and discover more high-dimensional manifold information to enhance the efficiency of feature extraction in the clustering tasks.
- (2) We develop an effective iterative algorithm based on multiplicative updating rules (MUR) to optimize the HGNTR model. Meanwhile, we apply the low-rank approximation trick to significantly reduce the computational complexity of HGNTR, which is called LraHGNTR.
- (3) Our experimental results show that both proposed algorithms can achieve higher performance metrics in clustering tasks, in addition, LraHGNTR can greatly reduce running time and even filter the noise from the original data.

The rest of this article is as follows: In Part 2, we firstly review the concepts and basic knowledge. In Part 3, we propose the HGNTR method and develop the MUR to update the model, and then develop the LraHGNTR. In Part 4, we take the different kinds of experiments to valid our method. The experimental results on the database prove the effectiveness of our theory. Part 5 is followed by the conclusion.

## 2. Notations and Preliminaries

We simply review the related notations and the definitions of nonnegative tensor decomposition as follows, and the basic notations are briefly reviewed in Table 1.

Table 1: The notations

Notations	Descriptions	Notations	Descriptions
$x$	A scalar	$\mathbf{x}$	A vector
$\mathbf{X}$	A matrix	$\mathcal{X}$	A tensor
$\ \cdot\ _F$	Frobenius norm	$\mathbf{I}$	Identity matrix
$\text{tr}\{\cdot\}$	Trace operation	$\otimes$	Kronecker product
$\times_n$	Mode- $n$ product	$\overline{\times}^1$	Multi-linear product

### 2.1. Definition

**Definition 1** (Mode- $n$  unfolding) Given a tensor  $\mathcal{X} \in \mathbb{R}^{I_1 \times I_2 \times \dots \times I_N}$ , its standard mode- $n$  unfolding matrix can be expressed as  $\mathbf{X}_{(n)} \in \mathbb{R}^{I_n \times I_1 \dots I_{n-1} I_{n+1} \dots I_N}$ , by fixing all the indices except  $I_n$  [18]. If we transform the unfolding matrix to the tensor, it is the inversion of the above operation and can be denoted as follow:

$$\mathcal{X} \leftarrow \text{folding}(\mathbf{X}_{(n)}).$$

The another mode- $n$  unfolding matrix of tensor  $\mathcal{X}$  is denoted by  $\mathbf{X}_{[n]} \in \mathbb{R}^{I_n \times I_{n+1} \dots I_N I_1 \dots I_{n-1}}$ , by fixing all the indices except  $I_n$ , which is often used in TR operations [19]. The distinction between two kinds of unfolding is the sequence of the  $N - 1$  indices.

**Definition 2** (Mode- $n$  product) The mode- $n$  product of a tensor  $\mathcal{X} \in \mathbb{R}^{I_1 \times I_2 \times \dots \times I_N}$  with a matrix  $\mathbf{U} \in \mathbb{R}^{J_n \times I_n}$  is denoted by  $\mathcal{X} \times_n \mathbf{U} \in \mathbb{R}^{I_1 \times \dots \times I_{n-1} \times J_n \times I_{n+1} \times \dots \times I_N}$ . See the [18] for the details. Element-wisely, we have the following formula:

$$(\mathcal{X} \times_n \mathbf{U})_{i_1 \dots i_{n-1} j_{i_{n+1}} \dots i_N} = \sum_{i_n=1}^{I_n} x_{i_1 i_2 \dots i_N} u_{j_{i_n} i_n}. \quad (1)$$

**Definition 3** (Multi-linear product) Given the tensor  $\mathcal{G}^{(n)} \in \mathbb{R}^{R_n \times I_n \times R_{n+1}}$  and  $\mathcal{G}^{(n+1)} \in \mathbb{R}^{R_{n+1} \times I_{n+1} \times R_{n+2}}$ , since the tensors  $\mathcal{G}^{(n)}$  and  $\mathcal{G}^{(n+1)}$  have an equivalent mode size  $R_{n+1}$ , they can be integrated into a single tensor by applying multi-linear product. And the single tensor can be denoted as  $\mathcal{G}^{(n,n+1)} \in \mathbb{R}^{R_n \times I_n I_{n+1} \times R_{n+2}}$  [20]. For multi-linear product, we have the following formula element-wisely:

$$\mathcal{G}_{r_n, (i_n-1) I_{n+1} + i_{n+1}, r_{n+2}}^{(n,n+1)} = \sum_{r_{n+1}=1}^{R_{n+1}} \mathcal{G}_{r_n, i_n, r_{n+1}}^{(n)} \mathcal{G}_{r_{n+1}, i_{n+1}, r_{n+2}}^{(n+1)}, \quad (2)$$

where  $i_n = 1, 2, \dots, I_n$  and  $i_{n+1} = 1, 2, \dots, I_{n+1}$ . For simplicity, it can be rewritten as:

$$\mathcal{G}^{(n,n+1)} = \mathcal{G}^{(n)} \overline{\times}^{-1} \mathcal{G}^{(n+1)}. \quad (3)$$

### 2.2. Nonnegative Tucker Decomposition

The nonnegative Tucker decomposition (NTD) make the tensor into the multiplication of nonnegative core tensor and factor matrices in tensor's each mode [21]. It can be written as follow:

$$\mathcal{A} = \mathcal{G} \times_1 \mathbf{A}^{(1)} \times_2 \mathbf{A}^{(2)} \dots \times_n \mathbf{A}^{(N)}, \quad (4)$$

where  $\mathcal{G} \in \mathbb{R}_+^{R_1 \times R_2 \times \dots \times R_N}$  denotes the nonnegative core tensor,  $\mathbf{A}^{(n)} \in \mathbb{R}_+^{I_n \times R_n}$ ,  $n = 1, 2, \dots, N$  denote the nonnegative factor matrices,  $\mathbf{A}^{(n)} \geq 0$ , and  $\mathcal{G} \geq 0$ . The  $\mathbf{R} = [R_1, R_2, \dots, R_N]$  is the nonnegative rank of NTD. However, the existence of the core tensor also increases the computation complexity of the model and limits the ability to represent higher-dimensional tensors.

### 2.3. Graph Regularized Nonnegative Tensor Ring Decomposition

Tensor ring (TR) decomposition is a more fundamental and general decomposition model than the Canonical Polyadic (CP) decomposition [22] and the Tucker decomposition (TD) [19]. The research results also proved

the model's effectiveness in various applications, e.g, tensor-based image completion [23, 24], hyperspectral image denoising [20], neural network compression [3, 25, 26], etc. Through the TR model, a high-order tensor  $\mathcal{X} \in \mathbb{R}^{I_1 \times I_2 \times \dots \times I_N}$  can be expressed as the circular contract products over a series of 3rd-order core tensors. Each element of the tensor  $\mathcal{X}$  can be written the as follow:

$$\mathcal{X}(i_1, i_2, \dots, i_N) = \text{Tr} \left\{ \prod_{n=1}^N \mathbf{G}_n(i_n) \right\}, \quad (5)$$

where  $\mathbf{G}_n(i_n) \in \mathbb{R}^{R_n \times R_{n+1}}$  is the  $i_n$ -th lateral slice matrix of the core tensor  $\mathcal{G}^{(n)} \in \mathbb{R}^{R_n \times I_n \times R_{n+1}}$ .  $\mathbf{R} = [R_1, R_2, \dots, R_N]$  is called TR-rank. The TR restricts the rank of the border core tensors to be equal, such as  $R_1 = R_{N+1}$ , not must be value-1, in other words, both border core tensors are 3rd-order tensors. Comparing with the Tensor Train decomposition (TT) [27] where the rank of edge core tensors  $R_1 = R_{N+1}$  must be restricted to value-1 and it can only keep relatively limited connection and interaction with between edge core tensors, the border core tensors of TR  $\mathcal{G}^{(1)}$  and  $\mathcal{G}^{(N)}$  can fully connect or interact each other directly enough. So TR can construct into a ring-like structure. Meanwhile, it is well known that the trace operations of matrices have cyclic invariance, such as  $\text{Tr}(ABC) = \text{Tr}(CAB)$ , and this property also holds for tensor ring decomposition. So the TR has the circular dimensional permutation invariance. These special attributes can make the TR model have some important numeric properties in the clustering task.

To further sufficiently learn local-parted information, Yu *et al.* proposed the Nonnegative Tensor Ring decomposition (NTR) [5]. The NTR is based on the TR model, it can be written as follow:

$$\begin{aligned} \min \frac{1}{2} \left\| \mathcal{X} - \text{NTR}(\mathcal{G}^{(1)}, \mathcal{G}^{(2)}, \dots, \mathcal{G}^{(N)}) \right\|_F^2 \\ \text{s.t. } \mathcal{G}^{(n)} \geq 0, \quad n = 1, 2, \dots, N, \end{aligned} \quad (6)$$

where  $\mathcal{G}^{(n)} \in \mathbb{R}_+^{R_n \times I_n \times R_{n+1}}$  denotes the  $n$ -th nonnegative core tensor.  $\text{NTR}(\mathcal{G}^{(1)}, \mathcal{G}^{(2)}, \dots, \mathcal{G}^{(N)})$  can be thought of as the reconstruction of the core tensors. The Frobenius norm is adopted to measure the similarity of them. According to the theorem 3.5 in [19], when we use alternating least squares (ALS) method, for the TR decomposition of  $\mathcal{X}$ , its matrix-form can be written as  $\mathbf{X}_{[n]} = \mathbf{G}_{(2)}^{(n)} \left( \mathbf{G}_{[2]}^{\neq n} \right)^\top$ . The central idea of ALS is to optimize a core tensor when the other core tensors are fixed, which has been extensively implemented in the CP decomposition and TD. Thus, the NTR problem (6) can be rewritten as the sub-problem framework:

$$\begin{aligned} \min \mathcal{F}_{NTR}^{(n)} = \frac{1}{2} \left\| \mathbf{X}_{[n]} - \mathbf{G}_{(2)}^{(n)} \left( \mathbf{G}_{[2]}^{\neq n} \right)^\top \right\|_F^2 \\ \text{s.t. } \mathbf{G}_{(2)}^{(n)} \geq 0, \quad n = 1, 2, \dots, N, \end{aligned} \quad (7)$$

where  $\mathbf{G}_{(2)}^{(n)} \in \mathbb{R}_+^{I_n \times R_n R_{n+1}}$  denotes the classical mode-2 unfolding matrix of  $\mathcal{G}^{(n)}$ .  $\mathbf{R} = [R_1, R_2, \dots, R_N]$  denotes nonnegative rank of NTR and  $\mathbf{G}_{[2]}^{\neq n} \in \mathbb{R}_+^{I_{n+1} \dots I_N I_1 \dots I_{n-1} \times R_n R_{n+1}}$  denotes the another type of mode-2 unfolding matrix of sub-chain tensor  $\mathcal{G}^{\neq n} \in \mathbb{R}_+^{R_{n+1} \times I_{n+1} \dots I_N I_1 \dots I_n \times R_n}$ . The sub-chain tensor  $\mathcal{G}^{\neq n}$  denotes the multi-linear product of all core tensors except the  $n$ -th core tensor and can be written as follow:

$$\mathcal{G}^{\neq n} = \mathcal{G}^{(n+1)} \overline{\times}^{-1} \dots \overline{\times}^{-1} \mathcal{G}^{(N)} \overline{\times}^{-1} \mathcal{G}^{(1)} \overline{\times}^{-1} \dots \overline{\times}^{-1} \mathcal{G}^{(n-1)}.$$

Detailed instructions about  $\mathcal{G}^{\neq n}$  can be found in the Definition 3.3 [19]. To enable NTR to observe the manifold geometrical structure of high-dimensional data, Yu *et al.* propose a graph regularized nonnegative tensor ring decomposition (GNTR) [5]. However, the learned graph from GNTR only models the single relationship between two objects, and therefore does not accurately indicate the high-dimensional manifold information.

#### 2.4. Hypergraph

The idea of hypergraph manifold learning is inspired by the theory of simple two-dimensional graph [12, 13]. In a normal graph, an edge is only connected with two vertices and the weight of the edge merely indicates the relationship between two connected vertices. However, in reality, the relationship of objects is more complex, there is a great possibility that there is a close connection between three vertices or more than. In this situation, the normal graph can not deal with this complex data well. The main distinction between hypergraph and normal two-order graph is that the hypergraph uses a subset of the vertices as an edge and each edge of a hypergraph usually connects more than two vertices. So the method of hypergraph manifold learning can promote the clustering performance [28–32]. Fig.1 is an example that shows the difference between hypergraph and normal graph.

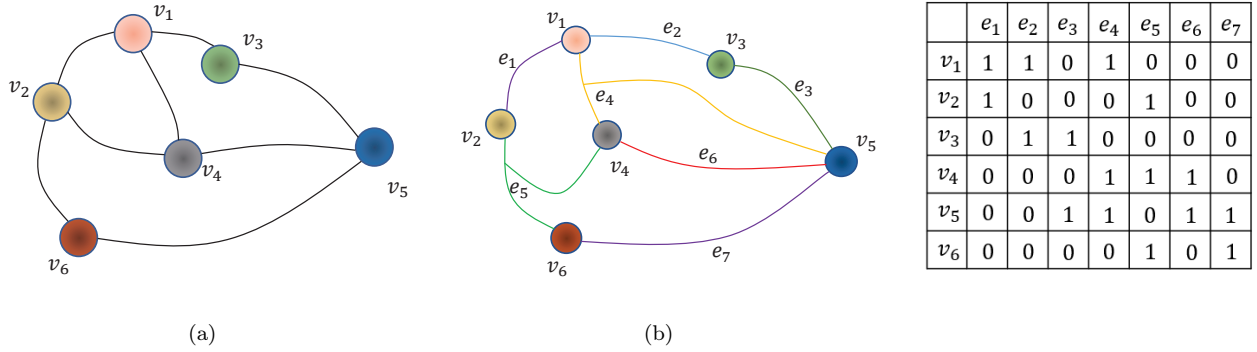


Figure 1: The difference between the hypergraph and normal graph. (a) A normal graph. (b) A hypergraph consists of the nodes and lines that denotes their relationships. (c) The incidence matrix  $\mathbf{H}$  of the hypergraph.

We assume that  $\mathbf{G} = (V, E, \mathbf{W})$  is a weighted hypergraph.  $V$  is a finite set of vertices in the hypergraph.  $E$  is the set of hyperedges. And each hyperedge  $e$  is a subset of  $V$ , then  $\cup_{e \in E} = V$ .  $\mathbf{W}$  is a diagonal matrix that represents the weights of hyperedge in which its elements are  $w$ .

The relationship of nodes and hyperedges in the hypergraph can be expressed by an indicator matrix  $\mathbf{H}$  with the size of  $|V| \times |E|$ . And the incidence matrix  $\mathbf{H}$  of hypergraph  $\mathbf{G}$  is defined as follows element-wisely [13]:

$$h(v, e) = \begin{cases} 1 & \text{if } v \in e \\ 0 & \text{if } v \notin e. \end{cases} \quad (8)$$

The affinity matrix  $\mathbf{A}$  of hypergraph is calculated as follow:

$$\mathbf{A}_{ij} = \exp\left(-\frac{\|v_i - v_j\|^2}{\sigma^2}\right). \quad (9)$$

where  $\sigma$  is the average distance,  $v_i$  and  $v_j$  denotes two vertices in the hypergraph. It denotes the probabilistic hypergraph [33]. It is important to note that since hypergraph can establish multiple connections among multiple vertices, they can learn a more stable and compact representation than normal graph. This special characteristic causes the hypergraph to be insensitive to hyper-parameters  $\sigma$ . And the weight matrix  $\mathbf{W}$  of hypergraph is calculated as follow:

$$\mathbf{W}_i = \sum_{v_j \in e_i} A(i, j). \quad (10)$$

The degree of hyperedge  $e$  with a symbol of  $d_E(e)$ , measures the amount of vertices or nodes  $v \in V$ , is defined as  $d_E(e) = \sum_{v \in V} h(v, e)$ . The degree of each vertex  $v \in V$  is the sum of weights for the hyperedges, is denoted as  $d_V(v) = \sum_{e \in E} w(e) h(v, e)$ . Here we denote  $\mathbf{D}_V$  as a diagonal matrix where its elements is  $d_V(v)$ . And  $\mathbf{D}_E$  can be denoted by a diagonal matrix where its elements is  $d_E(e)$ .

After obtaining a hypergraph that encodes the relationships among the samples, the data analysis tasks can be fulfilled by grouping the vertices in a way that measures the degree of similarity between samples, also known as hypergraph cutting missions from a graph learning perspective [11]. Then we can have the following hypergraph structure loss function:

$$\Omega = \frac{1}{2} \sum_{e \in E} \sum_{v_i, v_j \in e_i} \frac{w(e)h(v_i, e)h(v_j, e)}{d_E(e)} \left\| \frac{\mathbf{F}(v_i)}{\sqrt{d(v_i)}} - \frac{\mathbf{F}(v_j)}{\sqrt{d(v_j)}} \right\|_F^2, \quad (11)$$

where  $\mathbf{F} = [f_1, \dots, f_m]$  denotes the  $n \times m$  matrix. And  $f_i$  is a  $n$ -dimensional vector where each element indicates the probability that a vertex is a part of sub-graph. The Eq.(11) is designed to learn a set of hypergraph cuts that retain as many hyperedges as possible when partitioning. Notably, the sub-graphs are clusters of data after grouping. Thus, the complex data geometrical information can be preserved in the space of learned hypergraph cuts with much lower dimensionality than one of the sample spaces [34]. After a few steps of calculation [11], the Eq.(11) can be converted into a matrix form, as follows:

$$\begin{aligned} \Omega &= \text{tr} \{ \mathbf{F}^T (\mathbf{D}_v - \mathbf{H} \mathbf{W} \mathbf{D}_E^{-1} \mathbf{H}^T) \mathbf{F} \} \\ &= \text{tr} \{ \mathbf{F}^T \mathbf{L}_{hyper} \mathbf{F} \}, \end{aligned} \quad (12)$$

where  $\mathbf{L}_{hyper} = \mathbf{D}_v - \mathbf{S}$ , and  $\mathbf{S} = \mathbf{H} \mathbf{W} \mathbf{D}_E^{-1} \mathbf{H}^T$ .

### 3. Hypergraph Regularized Nonnegative Tensor Ring Factorization

In this part, in order to capture the multi-linear structural information and high-dimensional geometric manifold information of the data simultaneously, we innovatively add a hypergraph regularization term to the NTR model and propose the HGNTNTR model based on NTR decomposition. This model can express the original tensor data as a series of non-negative tensor circular contract products and completely capture the high-dimensional and complex manifold structural information. And we develop an effective algorithm to optimize the HGNTNTR model. At the same time, considering that the meaningful part of the data usually has a certain low-rank property, to reduce the computational complexity significantly, then we propose a low-rank approximation method (LraHGNTNTR).

### 3.1. Objective Function of HGNTN

Here we propose the hypergraph regularized NTR model, called HGNTN, to factorize the nonnegative tensors. And our goal is to use the hypergraph to learn the manifold information of the last dimension. It is also said that to learn the manifold structure of the last dimensional unfolding matrix if we write the HGNTN in the sub-problem framework. The reason is that in tensor data of our experimental database, the last dimension of data usually denotes the samples and defaults the number of objects, and the hypergraph regularized term is naturally imposed on the  $N$ -th core tensor. Given a tensor  $\mathcal{X} \in \mathbb{R}^{I_1 \times I_2 \times \dots \times I_N}$ , the objective function of HGNTN is as follows:

$$\begin{aligned} \min_{\mathbf{G}_{(2)}^{(n)}} \mathcal{F}_{HGNTN}^{(n)} &= \frac{1}{2} \left\| \mathbf{X}_{[n]} - \mathbf{G}_{(2)}^{(n)} \left( \mathbf{G}_{[2]}^{(n)} \right)^\top \right\|_F^2 + \frac{\beta}{2} \text{tr} \left( \left( \mathbf{G}_{(2)}^{(N)} \right)^\top \mathbf{L}_{hyper} \mathbf{G}_{(2)}^{(N)} \right) \\ \text{s.t. } \mathbf{G}_{(2)}^{(n)} &\geq 0, \quad n = 1, 2, \dots, N, \end{aligned} \quad (13)$$

in which the  $\mathbf{L}_{hyper} \in \mathbb{R}^{I_N \times I_N}$  is the hypergraph Laplacian matrices;  $\lambda \geq 0$  is a trade-off parameter to control the punishment of regularization term. *Fig.2* and *Fig.3* explain the principle and mechanism of HGNTN decomposition on ORL and GT database. The brief introduction of the databases is presented in Section 4.2. The last core tensor can be thought of as the feature tensor, and the other  $N - 1$  core tensors can be thought of as the basic tensors. By applying hypergraph regularization to the last core tensor, the higher-order similarity relations are preserved in the feature tensors that are decomposed by HGNTN.

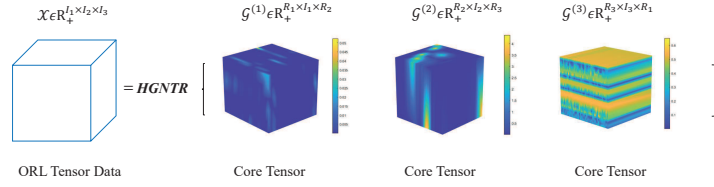


Figure 2: Illustration picture of HGNTN on three-order database. HGNTN decomposes the tensor into three core tensor, and expresses the information of each dimension as corresponding core tensor.

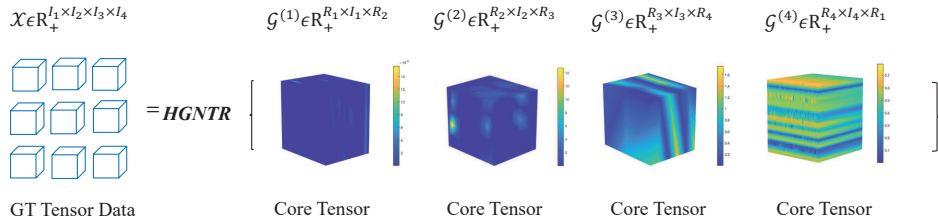


Figure 3: Illustration picture of HGNTN on four-order database. HGNTN decomposes the tensor into four core tensor, and expresses the information of each dimension as corresponding core tensor.



### 3.2. Optimization of HGNTTR

To solve the learned objective function in Eq.(13), we adopt the method of Multiplicative Updating Rules (MUR). Noticing that the equation  $\|\mathbf{A}\|_F^2 = \text{Tr}(\mathbf{A}\mathbf{A}^\top)$ , we define  $\mathbf{a}_{ik}$  as the Langrange multiplier for constraints  $\mathbf{G}_{(2)}^{(n)} \geq 0$ . And  $\mathbf{A} = [\mathbf{a}_{ik}]$ . The Langrange function  $\mathcal{L}_{HGNTTR}^{(n)}$  is as follow:

$$\begin{aligned} \mathcal{L}_{HGNTTR}^{(n)} = & \frac{1}{2} \text{tr} \left( \mathbf{X}_{[n]} (\mathbf{X}_{[n]})^\top - 2\mathbf{G}_{(2)}^{(n)} \left( \mathbf{G}_{[2]}^{\neq n} \right)^\top (\mathbf{X}_{[n]})^\top + \mathbf{G}_{(2)}^{(n)} \left( \mathbf{G}_{[2]}^{\neq n} \right)^\top \mathbf{G}_{[2]}^{\neq n} \left( \mathbf{G}_{(2)}^{(n)} \right)^\top \right) \\ & + \frac{\beta}{2} \text{tr} \left( \left( \mathbf{G}_{(2)}^{(n)} \right)^\top \mathbf{L}_{hyper} \mathbf{G}_{(2)}^{(n)} \right) + \text{Tr} \left( \mathbf{A} \left( \mathbf{G}_{(2)}^{(n)} \right)^\top \right). \end{aligned} \quad (14)$$

In the case of  $n = N$ , the derivatives of  $\mathcal{L}_{HGNTTR}^{(n)}$  with respect to  $\mathbf{G}_{(2)}^{(n)}$  is as follow :

$$\frac{\partial \mathcal{L}_{HGNTTR}^{(n)}}{\partial \mathbf{G}_{(2)}^{(n)}} = -\mathbf{X}_{[n]} \mathbf{G}_{[2]}^{\neq n} + \mathbf{G}_{(2)}^{(n)} \left( \mathbf{G}_{[2]}^{\neq n} \right)^\top \mathbf{G}_{[2]}^{\neq n} + \beta \left( \mathbf{G}_{(2)}^{(n)} \right)^\top \mathbf{L}_{hyper} + \mathbf{A}. \quad (15)$$

By using Karush-Kuhn-Tucker (KKT) condition, element-wisely  $\mathbf{a}_{ik} \left( \mathbf{G}_{(2)}^{(n)} \right)_{ik} = 0$ , we can get the follow update rules for each element in case of  $n = N$ :

$$\left( \mathbf{G}_{(2)}^{(n)} \right)_{ik} \leftarrow \left( \mathbf{G}_{(2)}^{(n)} \right)_{ik} \frac{\left( \mathbf{X}_{[n]} \mathbf{G}_{[2]}^{\neq n} + \beta \left( \mathbf{G}_{(2)}^{(n)} \right)^\top \mathbf{S} \right)_{ik}}{\left( \mathbf{G}_{(2)}^{(n)} \left( \mathbf{G}_{[2]}^{\neq n} \right)^\top \mathbf{G}_{[2]}^{\neq n} + \beta \left( \mathbf{G}_{(2)}^{(n)} \right)^\top \mathbf{D}_v \right)_{ik}}. \quad (16)$$

While  $n = 1, 2, \dots, N - 1$ , we just need to ignore the hypergraph regularized term. It is rewritten as follow:

$$\left( \mathbf{G}_{(2)}^{(n)} \right)_{ik} \leftarrow \left( \mathbf{G}_{(2)}^{(n)} \right)_{ik} \frac{\left( \mathbf{X}_{[n]} \mathbf{G}_{[2]}^{\neq n} \right)_{ik}}{\left( \mathbf{G}_{(2)}^{(n)} \left( \mathbf{G}_{[2]}^{\neq n} \right)^\top \mathbf{G}_{[2]}^{\neq n} \right)_{ik}}. \quad (17)$$

The whole algorithm procedure is given in Algorithm 1. Convergence can be proved by constructing auxiliary functions. The method is the same as the convergence proof in [8]. The valid experiment is designed to show the convergence property of HGNTTR and LraHGNTTR in section 4.7.

### 3.3. Fast HGNTTR Algorithm Based on Low-rank Approximation

In Eq.(16) and Eq.(17),  $\mathbf{X}_{[n]} \mathbf{G}_{[2]}^{\neq n}$  results in a large amount of computational complexity, especially in the condition of large-scale data. If  $\mathbf{X}_{[n]}$  can be replaced by a smaller term, it is possible to reduce the running time by a significant amount. Considering the well ability of Tucker decomposition (TD) [18] to approximate tensor data, and the fact that it also can decompose high-dimensional tensor into a series of low-rank factors, we choose the Tucker decomposition (TD) for the low-rank approximation.

The low-rank approximation has been successfully used in the field of matrix decomposition [35–37]. In the field of tensor, the fast tensor decomposition methods are proposed in [38], which are based on fiber sampling. Sequence extraction based on tSVD is also proposed in [39], which can achieve a balance between accuracy and efficiency. In addition, the theory of low-rank approximation has been applied to the NMF and NTF [16, 17], and the experiment

---

**Algorithm 1** HGNTNTR based on MU method
 

---

**Input:** Tensor  $\mathcal{X} \in \mathbb{R}^{I_1 \times I_2 \times \dots \times I_N}$ , nonnegative multi-way rank  $r_n$  for  $n = 1, 2, \dots, N$ , maximum number of iterations of  $t_{max}$ , balance parameter  $\beta$ , the number of nearest neighbours  $k$ .

**Output:** Core tensors  $\mathcal{G}_n$  for  $n = 1, 2, \dots, N$ .

- 1: Initialize  $\mathcal{G}_n \in \mathbb{R}^{R_n \times I_n \times R_{n+1}}$  for  $n = 1, 2, \dots, N$  as random tensors from the uniform distribution between 0 and 1.
  - 2: Calculate hypergraph Laplacian matrix  $\mathbf{L}_{hyper}$  by  $\mathbf{L}_{hyper} = \mathbf{D}_V - \mathbf{S}$ .
  - 3: **repeat**
  - 4:   **for**  $n = 1$  to  $N$  **do**
  - 5:     Obtain mode-2 unfolding matrix of sub-chain  $\mathbf{G}_{[2]}^{\neq n}$ .
  - 6:     **for**  $t = 1$  to  $t_{max}$  **do**
  - 7:       **if**  $n = N$  **then**
  - 8:         Updating  $\mathbf{G}_{(2)}^{(n)}$  and by Eq.(16).
  - 9:       **else**
  - 10:         Updating  $\mathbf{G}_{(2)}^{(n)}$  and by Eq.(17) .
  - 11:       **end if**
  - 12:     **end for**
  - 13:      $\mathcal{G}_n \leftarrow \text{folding}\left(\mathbf{G}_{(2)}^{(n)t_{max}}\right)$ .
  - 14:   **end for**
  - 15: **until** convergence
- 

results have demonstrated the effectiveness in reducing complexity and denoising. These methods can be used for dimensionality reduction of tensor data.

In this paper, we approximately change the original tensor  $\mathcal{X}$  into  $\tilde{\mathcal{X}}$  by the TD. Then the low-rank approximate term is used in iterative processes of HGNTNTR. We call this fast HGNTNTR algorithm the low-rank HGNTNTR (LraHGNTNTR).Details about denoising can be found in the section 4.5. The LraHGNTNTR can be explained as follows in two steps:

The low-rank approximation (LRA) step: obtain the LRA result of  $\mathcal{X}$  by normal Tucker decomposition (TD). It is denoted as follow:

$$\begin{aligned} \mathcal{X} &\approx \tilde{\mathcal{X}} = \left[ \mathcal{C}; \mathbf{U}^{(1)}, \mathbf{U}^{(2)}, \dots, \mathbf{U}^{(N)} \right] \\ &= \mathcal{C} \times_1 \mathbf{U}^{(1)} \times_2 \mathbf{U}^{(2)} \dots \times_N \mathbf{U}^{(N)}. \end{aligned} \tag{18}$$

the  $\mathcal{C}_+ \in \mathbb{R}_+^{\tilde{R}_1 \times \tilde{R}_2 \times \dots \times \tilde{R}_N}$  denotes Tucker core tensor, and  $\mathbf{U}^{(n)} \in \mathbb{R}_+^{I_n \times \tilde{R}_n}$ ,  $n = 1, 2, \dots, N$  denote factor matrices. Here,  $(\mathbf{U}^{(n)})^\top \mathbf{U}^{(n)} = \mathbf{I}$ . And  $\tilde{\mathbf{R}} = [\tilde{R}_1, \tilde{R}_2, \dots, \tilde{R}_N]$  is used to control the degree and error of approximation. The effect of rank  $\tilde{\mathbf{R}}$  on of the approximation accuracy will be described in detail in Section 4.4.

The NTR step: we need to perform NTR to minimize  $\frac{1}{2} \left\| \tilde{\mathcal{X}} - \text{NTR}(\mathcal{G}^{(1)}, \mathcal{G}^{(2)}, \dots, \mathcal{G}^{(N)}) \right\|_F^2$ . Now, we show how the derivatives computing of  $\mathcal{L}_{HGNTNTR}^{(n)}$  on  $\mathbf{G}_{(2)}^{(n)}$  can be accelerated after  $\mathcal{X}$  is replaced with its low-rank approximation  $\tilde{\mathcal{X}}$ . If the precondition exists, which tensor  $\mathcal{X}$  has not only the structure of Tucker, but also the structure of NTR,

we can have the following formula:

$$\begin{aligned}\tilde{\mathcal{X}} &= \mathcal{C} \times_1 \mathbf{U}^{(1)} \times_2 \mathbf{U}^{(2)} \dots \times_N \mathbf{U}^{(N)} \\ &\approx \text{NTR} \left( \mathcal{G}^{(1)}, \mathcal{G}^{(2)}, \dots, \mathcal{G}^{(N)} \right),\end{aligned}\quad (19)$$

where  $\mathcal{G}^{(n)} \in \mathbb{R}^{R_n \times I_n \times R_{n+1}}$ . Considering  $(\mathbf{U}^n)^\top \mathbf{U}^n = \mathbf{I}$ , we can get the following:

$$\mathcal{C} \approx \text{NTR} \left( \mathcal{G}^{(1)}, \mathcal{G}^{(2)}, \dots, \mathcal{G}^{(N)} \right) \times_1 \left( \mathbf{U}^{(1)} \right)^T \times_2 \left( \mathbf{U}^{(2)} \right)^T \times_3 \dots \times_N \left( \mathbf{U}^{(N)} \right)^T. \quad (20)$$

By storing  $\mathcal{C}$ ,  $\mathcal{G}$  and  $\mathbf{U}$  to reconstruct the approximation  $\tilde{\mathcal{X}}$ , we can consume much less computational complexity and storage especially when  $\tilde{R}_n \ll I_n$ . By the Theorem 4.2 in the [19], Eq.(20) can be rewritten as follow:

$$\begin{aligned}\mathcal{C} \times_n \mathbf{U}^{(n)} \\ \approx \text{NTR} \left( \mathcal{G}^{(1)} \times_2 \left( \mathbf{U}^{(1)} \right)^T, \dots, \mathcal{G}^{(n-1)} \times_2 \left( \mathbf{U}^{(n-1)} \right)^T, \mathcal{G}^{(n)}, \mathcal{G}^{(n+1)} \times_2 \left( \mathbf{U}^{(n+1)} \right)^T, \dots, \mathcal{G}^{(N)} \times_2 \left( \mathbf{U}^{(N)} \right)^T \right) \\ = \text{NTR} \left( \mathcal{Z}^{(1)}, \dots, \mathcal{Z}^{(n-1)}, \mathcal{G}^{(n)}, \mathcal{Z}^{(n+1)}, \dots, \mathcal{Z}^{(N)} \right),\end{aligned}\quad (21)$$

where  $\mathcal{Z}^{(n)} = \mathcal{G}^{(n)} \times_2 \left( \mathbf{U}^{(n)} \right)^T \in \mathbb{R}^{R_n \times \tilde{R}_n \times R_{n+1}}$ ,  $n = 1, \dots, n-1, n+1, \dots, N$ . The term  $\mathbf{X}_{[n]} \mathbf{G}_{[2]}^{\neq n}$  can be written as follow:

$$\begin{aligned}\mathbf{X}_{[n]} \mathbf{G}_{[2]}^{\neq n} \\ \approx \mathbf{U}^{(n)} \mathbf{C}_{(n)} \left( \mathbf{U}^{\neq n} \right)^T \mathbf{G}_{[2]}^{\neq n} \\ = \mathbf{U}^{(n)} \mathbf{C}_{(n)} \mathbf{Z}_{[2]}^{\neq n}.\end{aligned}\quad (22)$$

where  $\mathbf{C}_{(n)} \in \mathbb{R}^{\tilde{R}_n \times \tilde{R}_1 \dots \tilde{R}_{n-1} \tilde{R}_{n+1} \dots \tilde{R}_N}$  is the mode- $n$  unfolding matrix of  $\mathcal{C}$  and  $\mathbf{Z}_{[2]}^{\neq n} \in \mathbb{R}^{\tilde{R}_{n+1} \dots \tilde{R}_N \tilde{R}_1 \dots \tilde{R}_{n-1} \times R_n R_{n+1}}$  denotes the mode-2 unfolding matrix of sub-chain tensor  $\mathcal{Z}^{\neq n}$ .  $\mathcal{Z}^{\neq n}$  and  $\mathbf{U}^{\neq n}$  is defined as follow:

$$\begin{aligned}\mathcal{Z}^{\neq n} &= \mathcal{Z}^{(n+1)} \overline{\times}^{-1} \dots \overline{\times}^{-1} \mathcal{Z}^{(N)} \overline{\times}^{-1} \mathcal{Z}^{(1)} \overline{\times}^{-1} \dots \overline{\times}^{-1} \mathcal{Z}^{(n-1)}, \\ \mathbf{U}^{\neq n} &= \left[ \mathbf{U}^{(N)} \otimes \dots \otimes \mathbf{U}^{(n+1)} \otimes \mathbf{U}^{(n-1)} \otimes \dots \otimes \mathbf{U}^{(1)} \right]^T.\end{aligned}$$

Finally, we need to change the  $\mathbf{X}_{[n]} \mathbf{G}_{[2]}^{\neq n}$  by Eq.(22). And we can get the following update rules for each element in case of  $n = N$ :

$$\left( \mathbf{G}_{(2)}^{(n)} \right)_{ik} \leftarrow \left( \mathbf{G}_{(2)}^{(n)} \right)_{ik} \frac{\left( \mathbf{U}^{(n)} \mathbf{C}_{(n)} \mathbf{Z}_{[2]}^{\neq n} + \beta \left( \mathbf{G}_{(2)}^{(n)} \right)^\top \mathbf{S} \right)_{ik}}{\left( \mathbf{G}_{(2)}^{(n)} \left( \mathbf{G}_{[2]}^{\neq n} \right)^\top \mathbf{G}_{[2]}^{\neq n} + \beta \left( \mathbf{G}_{(2)}^{(n)} \right)^\top \mathbf{D}_v \right)_{ik}}. \quad (23)$$

While  $n = 1, 2, \dots, N-1$ , the update rules are rewritten as follow:

$$\left( \mathbf{G}_{(2)}^{(n)} \right)_{ik} \leftarrow \left( \mathbf{G}_{(2)}^{(n)} \right)_{ik} \frac{\left( \mathbf{U}^{(n)} \mathbf{C}_{(n)} \mathbf{Z}_{[2]}^{\neq n} \right)_{ik}}{\left( \mathbf{G}_{(2)}^{(n)} \left( \mathbf{G}_{[2]}^{\neq n} \right)^\top \mathbf{G}_{[2]}^{\neq n} \right)_{ik}}. \quad (24)$$

The whole LraHGNTR algorithm is given in Algorithm 2.

---

**Algorithm 2** LraHGNTR based on MU method

---

**Input:** Tensor  $\mathcal{X} \in \mathbb{R}^{I_1 \times I_2 \times \dots \times I_N}$ , nonnegative multi-way rank  $r_n$  for  $n = 1, 2, \dots, N$ , multi-linear rank  $\tilde{\mathbf{R}}_n$ , maximum number of iterations of  $t_{max}$ , balance parameter  $\beta$ , the number of nearest neighbours  $k$ .

**Output:** Core tensors  $\mathcal{G}_n$  for  $n = 1, 2, \dots, N$ .

- 1: Initialize  $\mathcal{G}_n \in \mathbb{R}^{R_n \times I_n \times R_{n+1}}$  for  $n = 1, 2, \dots, N$  as random tensors from the uniform distribution between 0 and 1.
  - 2: Calculate hypergraph Laplacian matrix  $\mathbf{L}_{hyper}$  by  $\mathbf{L}_{hyper} = \mathbf{D}_V - \mathbf{S}$ .
  - 3: **repeat**
  - 4:   **for**  $n = 1$  to  $N$  **do**
  - 5:     Obtain the sub-chain tensor  $\mathcal{Z}^{\neq n}$ .
  - 6:     **for**  $t = 1$  to  $t_{max}$  **do**
  - 7:       **if**  $n = N$  **then**
  - 8:         Updating  $\mathbf{G}_{(2)}^{(n)}$  by Eq.(23).
  - 9:       **else**
  - 10:         Updating  $\mathbf{G}_{(2)}^{(n)}$  by Eq.(24).
  - 11:       **end if**
  - 12:     **end for**
  - 13:      $\mathcal{G}_n \leftarrow \text{folding}\left(\mathbf{G}_{(2)}^{(n)t_{max}}\right)$ .
  - 14:   **end for**
  - 15: **until** convergence.
- 

### 3.4. Computational Complexity Analysis

The HGNTR is efficiently updated by the method of Multiplicative Updating Rule. To simplify, we assume that  $I = I_n$  and  $R = R_n R_{n+1}$ ,  $n = 1, 2, \dots, N$ . For the each iteration of the HGNTR algorithm, the tensor  $\mathcal{G}^{\neq n}$  is calculated and its computational cost is  $\mathcal{O}_{\mathcal{G}^{\neq n}} = (I^2 + I^3 + \dots + I^{N-1})R^{\frac{3}{2}}$ . It is important to note that we do not need to compute  $\left(\mathbf{G}_{[2]}^{\neq n}\right)^\top \mathbf{G}_{[2]}^{\neq n}$  explicitly, instead, we just use the self-contraction operation for each small core tensors  $\mathcal{G}^{(n)}$ ,  $n = 1, 2, \dots, n = N - 1$  in sequential order, then compute their product. The similar approaches has been used for CP and Tucker decomposition. By this operation, the computational complexity of  $\left(\mathbf{G}_{[2]}^{\neq n}\right)^\top \mathbf{G}_{[2]}^{\neq n}$  is changing from  $(I^{N-1})R^2$  to  $(N - 1)IR^2 + (N - 2)R^3$ . We can conclude that as the dimension increases, the computational complexity increases linearly, making this operation more useful to represent higher-order tensor data such as four-order or more.

The total computational complexity of HGNTR in case of  $n = 1, 2, \dots, N - 1$  is  $\mathcal{O}_{\mathcal{G}^{\neq n}} + \mathcal{O}((I^N R + IR + IR^2 + (N - 1)IR^2 + (N - 2)R^3))$ . In the case of  $n = N$ , the HGNTR only adds the cost of calculating the graph regularization term. As a result of the  $\mathbf{L}_{hyper}$  is usually sparse, the computational complexity of the hypergraph term is small. Then the computational cost of HGNTR is  $\mathcal{O}_{\mathcal{G}^{\neq n}} + \mathcal{O}(I^N R + IR + IR^2 + (N - 1)IR^2 + (N - 2)R^3 + 2I^2 R)$ .

For the LraHGNTR, we assume that  $I = I_n$  and  $\tilde{R} = \tilde{R}_n \tilde{R}_{n+1}$ ,  $n = 1, 2, \dots, N$ . The computing complexity of the mode-2 product of core tensors and factor matrices in Eq.(21) is  $\mathcal{O}_M = (N - 1)\tilde{R}RI$ . The total computational complexity of LraHGNTR in case of  $n = 1, 2, \dots, N - 1$  is  $\mathcal{O}_M + \mathcal{O}(I(\tilde{R}^{N-1}(R + \tilde{R})) + IR^2 + IR + (N - 1)IR^2 + (N - 2)R^3)$ . In the case of  $n = N$ , the total computational cost of LraHGNTR is  $\mathcal{O}_M + \mathcal{O}(I(\tilde{R}^{N-1}(R + \tilde{R})) + IR^2 +$

$$2I^2R + IR + (N - 1)IR^2 + (N - 2)R^3).$$

The Table 2 shows the total floating-point counts of HGNTR and LraHGNTNTR in detail when updating. From the above complexity analysis, we can conclude that, when the data size is large, and  $R = \tilde{R}_n \ll I$ , the computational complexity is greatly reduced and the speed of LraHGNTNTR is significantly ahead.

Algorithm	HGNTR	LraHGNTNTR
Addition	$NI^N R + NIR^2 +$ $N(N - 1)IR^2 + 2IR$ $2I^2R + N(N - 2)R^3$	$NI(\tilde{R}^{N-1}(R + \tilde{R})) + 2IR$ $NIR^2 + N(N - 1)IR^2$ $+N(N - 2)R^3 + 2I^2R$
Multiplication	$NI^N R + NIR^2 + NIR +$ $+N(N - 1)IR^2$ $+2I^2R + N(N - 2)R^3$	$NI(\tilde{R}^{N-1}(R + \tilde{R})) + NIR +$ $NIR^2 + N(N - 1)IR^2$ $+N(N - 2)R^3 + 2I^2R$
Division	$NIR$	$NIR$
Overall	$\mathcal{O}(NI^N R)$	$\mathcal{O}\left(NI(\tilde{R}^{N-1}(R + \tilde{R}))\right)$

Table 2: Computational operation floating-point counts of HGNTR and LraHGNTNTR for each iteration when updating.

## 4. Experiment

In this section, we firstly introduce performance metrics such as accuracy (ACC), normalized mutual information (NMI), and purity (PUR). Then we simply review the databases that are used for our experiment. We select six proposed algorithms as the comparison in the experiments to prove our model effectiveness. We do clustering experiments to count the performance metrics of our algorithm on different datasets. After that, we test the accuracy of the noisy-added database. Finally, we will do the parameter sensitivity experiment and convergence experiment to test the robustness and stability of HGNTR and LraHGNTNTR. And we make the basic visualization to verify our excellent performance of clustering again.

### 4.1. Performance Metrics

To evaluate the effectiveness of each algorithm, we adopt three metrics such as ACC, NMI, and PUR. The definition of ACC is as follows:

$$\text{ACC}(y_i, \hat{y}_i) = \frac{1}{n} \sum_{i=1}^n \delta(y_i, \text{map}(\hat{y}_i)),$$

where  $n$  is the total amount of objects of database.  $y_i$  and  $\hat{y}_i$  respectively denotes the cluster label of the object and the true label of the object.  $\text{map}(\cdot)$  denotes the permutation mapping function, which is responsible for mapping each cluster label  $y_i$  to the equivalent label of the database.  $\delta(\cdot)$  is the delta function. The AC is used to measure how similar the true label and the experiment-got label. For example, if the object label  $y_i$  and the real label  $\hat{y}_i$  are equal, then  $(y_i, \text{map}(\hat{y}_i)) = 1$ , if not, then  $(y_i, \text{map}(\hat{y}_i)) = 0$ .

By combining with the information theory, the agreement between two cluster parts can be measured with mutual information (MI). The MI is widely used in clustering applications. MI between the two sets of cluster labels  $C'$  and true labels  $C$  is defined by

$$\text{MI}(C, C') = \sum_{c_i \in C, c'_i \in C'} p(c_i, c'_i) \cdot \log_2 \frac{p(c_i, c'_i)}{p(c_i) \cdot p(c'_i)},$$

in which  $p(c_i)$  and  $p(c'_i)$  denote the probability that the object that is selected arbitrarily from the databases belongs to of category  $c_i$  and category  $c'_i$ . And  $p(c_i, c'_i)$  is defined as the joint probability that object belongs to category  $c_i$  and category  $c'_i$  at the same time. To force the score to have an upper bound, we use the NMI as one of evaluation measures and the definition of NMI is denoted as follows:

$$\text{NMI}(C, C') = \frac{\text{MI}(C, C')}{\max(H(C), H(C'))},$$

where  $H(C)$  and  $H(C')$  are defined as the entropies of the true label set  $C$  and the cluster label set  $C'$ . It is obvious to know the score ranges of  $\text{NMI}(C, C')$  is from 0 to 1. If the two label sets are the same, the  $\text{NMI}(C, C') = 1$ , otherwise  $\text{NMI}(C, C') = 0$ .

The PUR measures the degree that how many each cluster contains data points are from single category. Given a certain category  $C_i$  which size is  $n_i$ , the definition of PUR is as follows [40]:

$$\text{PUR}(C_i) = \frac{1}{n_i} \max_h (n_i^h),$$

where  $\max_h (n_i^h)$  is the number that represents the number of categories from category  $C_i$  belongs to category  $h$ .

#### 4.2. Databases

In the experiment, we use two databases to prove the effectiveness of our method. A brief introduction of the two databases is as follows:

- **ORL Database:** The ORL face database contains 400 grey-scale images of 40 different individuals. For the image in each category, these images are collected in a different light, facial expressions, and facial details. All the images are taken against a dark, uniform background, and the front face. In this experiment, each image is adjusted to the size of  $32 \times 27$ . We construct a 3rd-order tensor  $\mathcal{X} \in \mathbb{R}^{32 \times 27 \times 400}$ .
- **GT Database:** The Georgia Tech face database contains images of 50 people. All people in the database are represented by 15 color images with a cluttered background that is taken at resolution  $640 \times 480$  pixels. The average size of the faces in these images is  $150 \times 150$  pixels. The pictures show frontal or tilted faces with different facial expressions, lighting conditions, and scales. We downsampled every image to  $40 \times 30 \times 3$ , finally we get the 4rd-order tensor  $\mathcal{X} \in \mathbb{R}^{40 \times 30 \times 3 \times 750}$ .
- **Face95 Database:** The Face95 dataset consists of color facial images, represented by 72 individuals, each with 20 exclusive images. Hence, there are 1440 face images in the dataset. The dataset contains frontal faces with mild expressions. We downsampled the database to  $50 \times 40 \times 3$ , finally we get the 4rd-order tensor  $\mathcal{X} \in \mathbb{R}^{50 \times 40 \times 3 \times 1000}$ .

- Face96 Database: The facial images in the Face96 dataset are full color and consist of 152 individuals, each with 20 images. Therefore, there are 3040 images in the dataset. All faces in this dataset have complicated backgrounds comparing to ORL and Face95. Furthermore, the images were taken under various lighting situations and the faces contain different ranges of expressions. We downsampled every image to  $49 \times 49 \times 3$ , finally we get the 4rd-order tensor  $\mathcal{X} \in \mathbb{R}^{49 \times 49 \times 3 \times 1200}$ .

#### 4.3. Comparison Algorithms

In order to ensure the fairness of the experiment, our algorithms all use Multiplicative Updating (MU) rules to update the model. To verify the effectiveness of our proposed algorithms, we compare our algorithms with the following state-of-the-art algorithms in our tasks.

- K-means: One of the most famous unsupervised clustering algorithms.
- NMF: Nonnegative matrix factorization aims to learn the parts-based basis of data objects [1].
- GNMF: Graph regularized nonnegative matrix factorization (GNMF), the NMF considering the manifold geometric structure in the data [8].
- HNMF: Hypergraph regularized nonnegative matrix factorization (HNMF), the NMF considering the high-dimensional manifold geometric structure in the data [12].
- NTR-MU: Nonnegative tensor ring decomposition based on MU optimization rule to learn the parts-based basis of tensor data objects [5].
- GNTR-MU: Graph regularized nonnegative tensor ring decomposition based on MU optimization rule, the NTR considering the manifold geometric structure in the data [5].

#### 4.4. Clustering Tasks for Real-world Database

In this part of the experiment, we test the comprehensive clustering performance of extracted low-dimensional features of our proposed algorithms HGNTR and LraHGNTNTR on databases, including their subsets. The method of getting subsets is that we randomly select the partial  $n$  samples from each database and merge  $n$  samples as a subset of each database. Considering the number of categories, we divide the ORL into  $k_{ORL} \in \{10, 15, 20, 25, 30, 35, 40\}$  categories. We divide the GT into  $k_{GT} \in \{10, 20, 30, 40, 50\}$  categories. We divide the Face95 into  $k_{Face95} \in \{10, 20, 30, 40, 50\}$  categories. We divide the Face96 into  $k_{Face96} \in \{20, 30, 40, 50, 60\}$  categories. Meanwhile, while running the matrix methods such as NMF, GNMF, HNMF, we need to transform the tensor into the matrix by the Matlab reshape operation. All the experiments are performed on a personal computer with an i5-9500T at 2.20GHz, 16GB memory, Windows 10, and Matlab 2020b. For the ORL, the maximum number of iterations is set to 10. For the other databases, maximum number of iterations is set to 5. We have counted the ACC, NMI, PUR, and their STDs obtained from the experimental results in Table 3, Table 4, Table 5, and Table 6. Through the experimental results, we can get the following conclusions:

- For the matrix method, the effectiveness of HNMF is usually better than that of GNMF and NMF, indicating that the manifold information obtained by our hypergraph regularization can better reflect the complex manifold geometry information of the data. And it also can help improve the recognizability of low-dimensional character. Meanwhile, we have also observed that with the growth of sample categories, in other words, the amount of data, HNMF shows limited ability to obtain hypergraph information. It proves the necessity that we need to develop the tensor method of manifold learning that is more suitable for high-dimensional data.
- GNTR is usually better than NTR, shows that the learned manifold geometry can effectively enhance the identifiability of low-dimensional features. HGNTNTR is usually better than HNMF, indicating that our algorithm HGNTNTR can learn low-dimensional features better by learning spatial structure information in the form of tensors.
- HGNTNTR is usually better than general other algorithms, which illustrates the model in which tensor learning algorithm and hypergraph are combined together, can learn the complex structure information, comparing with the state-of-the-art methods. Hypergraph is an effective method, it can find more than two connection relationships between data points. It can improve the accuracy of clustering.
- When the data volume (number of categories) of the three datasets is small, we find that sometimes the performance metrics of tensor methods are a little weaker than matrix methods. The reason is that tensor methods are more effective in the condition of larger amounts of data. It also reflects the advantages of the tensor approaches.

We also count the running time of each database under different categories in *Fig.4*. Through the experimental results, we can get the following conclusions:

- Noting that the question of running time of HGNTNTR and the computational complexity, we consider using a low-rank Tucker approximation method to replace the greatly complex term in the iterative process. Experiments have shown that the performance of HGNTNTR and LraHGNTNTR are similar, but LraHGNTNTR can greatly reduce the running time. It verifies that the low-rank Tucker approximation can effectively reduce the computational cost while retaining the accuracy. This is a key point of our algorithm leading other algorithms.
- Through the comparison of subsets, we also found that as the category of subsets increases, in other words, as the number of data increases, compared with other algorithms, our algorithm HGNTNTR and LraHGNTNTR outperforms more obviously. Especially for LraHGNTNTR, as the amount of data increases, the performance of our algorithm LraHGNTNTR drops significantly in the running time.

By the experiment, we can conclude that the effect of rank  $\tilde{\mathbf{R}}$  for LraHGNTNTR, if we choose a lower rank, our running time will be greatly reduced, but the accuracy will be lost. If we choose a little larger rank, our accuracy will increase. So if we choose a suitable rank, we can retain the accuracy, and get the ideal running time.



	$k_{ORL}$	K-means	NMF	GNMF	HNMF	NTR-MU	GNTR-MU	HGNTR-MU	lraHGNTR-MU
ACC	10	75.80±3.35	77.70±3.26	74.60±2.87	75.30±3.40	71.70±2.75	78.00±2.70	<b>78.30±3.49</b>	<u>78.10±3.14</u>
	15	69.93±2.97	75.06±5.57	73.80±4.48	76.33±4.01	68.53±4.80	75.40±2.40	<b>77.06±3.37</b>	<u>76.66±2.96</u>
	20	69.60±3.31	72.55±2.99	75.15±2.69	78.85±3.85	70.00±2.69	78.00±4.18	<u>80.05±2.87</u>	<b>80.10±2.99</b>
	25	68.64±4.24	72.80±4.58	76.12±2.34	75.90±3.05	68.60±3.08	77.64±2.66	<u>80.68±3.69</u>	<b>81.20±2.95</b>
	30	73.36±2.66	69.36±2.66	73.80±2.41	72.96±3.39	66.16±4.91	73.60±2.66	<u>74.00±2.51</u>	<b>76.06±2.21</b>
	35	66.54±4.69	69.08±2.43	72.85±2.30	72.32±2.15	63.71±2.97	73.65±2.54	<b>74.08±1.60</b>	<u>73.91±2.87</u>
	40	66.95±3.54	67.93±2.01	73.28±2.77	71.47±2.73	68.55±3.43	74.70±2.85	<u>75.65±2.09</u>	<b>76.55±2.10</b>
NMI	10	85.54±1.06	84.19±2.24	84.71±1.32	84.78±0.82	80.74±3.43	84.07±1.31	<u>85.40±1.06</u>	<b>85.22±0.78</b>
	15	84.13±1.47	85.30±3.55	85.59±1.99	<u>88.11±1.65</u>	80.79±1.76	86.22±1.30	87.94±1.52	<b>87.93±1.15</b>
	20	82.99±2.08	84.03±2.21	85.60±1.86	88.12±2.46	83.05±2.04	87.36±1.62	<u>89.15±0.95</u>	<b>89.18±1.72</b>
	25	84.62±1.71	85.40±2.75	87.38±1.67	87.81±1.05	82.79±1.78	87.35±0.80	<u>89.98±1.20</u>	<b>90.06±0.96</b>
	30	84.13±1.77	84.46±1.55	87.20±0.76	87.02±1.35	82.78±2.37	87.36±0.99	<u>88.20±1.25</u>	<b>88.76±0.84</b>
	35	83.87±2.17	85.13±1.18	86.55±1.42	87.13±1.21	80.89±1.61	87.02±1.15	<u>88.06±1.01</u>	<b>88.11±0.91</b>
	40	84.59±1.43	84.08±0.68	87.78±1.07	87.44±0.98	84.78±1.65	88.51±0.77	<u>89.81±1.07</u>	<b>89.91±0.73</b>
PUR	10	80.10±2.60	80.70±2.45	78.90±1.59	79.90±2.96	75.30±3.26	81.30±1.41	<u>81.60±2.01</u>	<b>81.70±2.05</b>
	15	76.06±2.34	79.33±4.71	79.33±3.23	81.40±2.72	72.20±2.86	80.53±1.62	<u>81.66±2.49</u>	<b>81.73±1.87</b>
	20	73.30±3.09	76.10±3.06	78.25±2.72	81.55±3.70	73.85±2.82	80.75±3.29	<u>82.65±1.90</u>	<b>82.50±2.83</b>
	25	73.64±3.36	76.40±3.77	79.20±1.98	79.04±1.96	72.12±2.83	80.12±2.00	<u>82.88±2.69</u>	<b>83.28±1.70</b>
	30	71.60±3.30	73.36±2.66	76.96±2.07	76.43±2.72	74.23±3.45	77.20±1.91	<u>77.46±2.05</u>	<b>78.96±1.95</b>
	35	70.97±3.46	72.94±2.28	75.83±2.32	76.17±1.64	67.45±2.92	76.54±1.96	<u>76.74±2.12</u>	<b>77.45±2.07</b>
	40	71.33±2.95	71.53±0.76	76.83±2.03	75.47±1.78	72.95±2.87	78.30±1.92	<u>79.45±1.52</u>	<b>79.65±2.00</b>

Table 3: Performance metrics comparisons on ORL database between K-means, NMF, GNMF, HNMF, NTR-MU, GNTR-MU, HGNTR-MU and LraHGNTR-MU methods. We divide the database into different subset. Each subset contains  $k_{ORL}$  categories.

#### 4.5. Clustering Tasks for Real-world Database with Gaussian Noise

In this part, we count the performance of our algorithm on the noisy dataset. In the case of noiseless, we can easily find that LraHGNTR is similar to HGNTR in accuracy, but LraHGNTR is faster. We compare various algorithm performances by adding the Gaussian noise on ORL and GT database. The degree of noise is measured by the signal-to-noise ratio (SNR). Before the experiment, as a result of the negative value may appear in datasets after adding very heavy Gaussian noise, we make the negative value in each database are truncated at zero to ensure the negativity for each algorithm except LraHGNTR. The reason is that LraHGNTR can directly deal with non-negative elements. The Fig.6, Fig.7, Fig.8 and Fig.9 show the comparison with noise. Through experiment results, we can get the following conclusions:

- For the datasets with adding Gaussian noise, our algorithms can still achieve good results compared with other

	$k_{GT}$	K-means	NMF	GNMF	HNMF	NTR-MU	GNTR-MU	HGNTR-MU	lraHGNTR-MU
ACC	10.00	62.66±2.49	66.40±3.07	62.13±3.31	67.33±2.44	62.66±3.36	<u>74.80±4.09</u>	74.00±2.49	<b>75.33±2.90</b>
	20.00	53.20±4.97	54.80±1.82	46.53±4.18	54.33±0.62	57.33±4.23	61.26±2.03	<u>61.53±0.93</u>	<b>62.66±3.30</b>
	30.00	46.48±2.67	48.27±1.70	43.91±2.24	49.06±0.92	48.53±6.14	53.78±2.29	<u>58.22±2.48</u>	<b>59.02±1.81</b>
	40.00	46.47±0.85	47.26±2.57	45.76±0.38	48.50±1.56	53.90±8.34	52.70±1.03	<u>55.37±2.49</u>	<b>55.80±1.55</b>
	50.00	45.71±0.76	45.72±1.16	43.33±1.80	49.49±1.20	43.47±6.21	50.80±2.86	<u>52.00±2.37</u>	<b>53.25±2.33</b>
NMI	10.00	72.76±2.74	72.97±2.30	68.06±2.74	69.00±3.09	66.45±1.77	74.25±3.79	<u>74.69±2.70</u>	<b>75.55±1.64</b>
	20.00	66.99±3.01	65.97±1.67	58.30±3.96	66.81±1.17	67.42±3.68	71.89±1.97	<u>73.01±0.87</u>	<b>73.04±2.10</b>
	30.00	62.21±0.92	63.50±2.17	59.33±1.63	63.57±0.80	64.45±5.05	67.70±0.62	<u>70.85±1.32</u>	<b>71.51±0.91</b>
	40.00	63.26±0.83	63.54±1.39	62.98±0.84	65.06±0.93	68.69±5.55	68.71±0.41	<b>71.24±0.76</b>	<u>70.82±0.65</u>
	50.00	64.37±0.58	63.64±0.48	62.76±1.58	66.12±0.86	63.30±5.52	69.25±2.31	<u>70.64±2.23</u>	<b>71.42±2.30</b>
PUR	10.00	66.26±3.60	69.60±2.64	64.93±2.38	67.46±2.68	64.66±3.62	<u>74.80±4.09</u>	74.53±2.23	<b>76.13±1.52</b>
	20.00	56.87±3.73	57.47±1.72	49.33±3.74	57.73±1.48	60.67±3.66	64.60±2.01	<u>64.86±0.98</u>	<b>65.06±3.18</b>
	30.00	49.38±2.07	50.89±2.07	46.67±1.84	52.35±1.06	52.08±6.55	57.37±2.30	<u>61.11±1.72</u>	<b>61.86±1.09</b>
	40.00	49.20±0.43	50.00±2.57	48.03±0.55	51.33±1.75	56.73±7.16	55.93±0.75	<u>58.36±2.07</u>	<b>59.10±1.13</b>
	50.00	48.24±0.92	47.78±1.26	46.48±2.02	51.65±1.23	46.43±6.79	54.49±2.98	<u>55.49±2.38</u>	<b>56.16±2.98</b>

Table 4: Performance metrics comparisons on GT database between K-means, NMF, GNMF, HNMF, NTR-MU, GNTR-MU, HGNTR-MU and LraHGNTR-MU methods. We divide the database into different subset. Each subset contains  $k_{GT}$  categories.

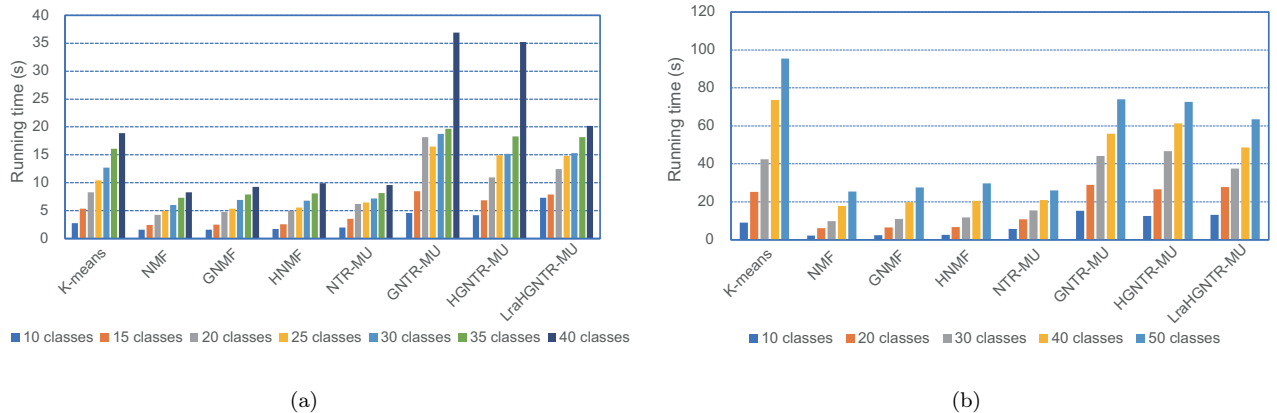


Figure 4: The running time of various algorithms subset in different number of categories. (a) ORL. (b) GT.

algorithms, and the running time of LraHGNTR is also reduced. It proves the effectiveness of our algorithms again.

- In the case of mild noise, our approximate algorithm LraHGNTR can achieve almost the same performance as the HGNTR. And in the case of high noise, such as  $SNR = 10\text{ dB}$ , the LraHGNTR is obviously better than HGNTR, which demonstrates that the low-rank approximation method is beneficial to filter noise.

	$k_{Face95}$	K-means	NMF	GNMF	HNMF	NTR-MU	GNTR-MU	HGNTR-MU	lraHGNTR-MU
ACC	10	76.50±6.76	79.20±4.20	84.90±1.51	82.40±5.09	73.40±4.76	85.20±2.41	<u>85.60±2.10</u>	<b>86.10±2.56</b>
	20	59.05±1.67	58.10±2.82	65.50±1.74	60.40±3.92	56.45±1.68	64.05±4.66	<u>64.80±4.42</u>	<b>66.00±0.53</b>
	30	50.96±3.47	49.53±1.70	54.73±1.69	55.60±1.42	51.66±1.53	55.06±1.78	<b>56.50±1.87</b>	<u>56.30±2.62</u>
	40	47.90±3.10	45.70±1.90	50.00±1.40	49.25±2.06	46.02±1.61	50.17±1.80	<u>50.58±1.96</u>	<b>51.43±1.83</b>
	50	44.82±1.99	44.18±1.38	49.24±1.20	46.20±2.65	45.74±1.54	49.68±1.57	<b>51.02±2.11</b>	<u>50.48±1.89</u>
NMI	10	79.67±2.88	78.58±3.59	83.55±1.62	84.07±1.74	74.78±1.69	83.48±1.89	<u>84.20±2.37</u>	<b>85.04±2.45</b>
	20	70.64±1.34	69.52±0.94	73.71±1.00	71.66±1.78	67.95±0.93	<b>74.85±2.77</b>	74.00±1.88	<u>74.39±0.53</u>
	30	68.53±2.26	67.18±0.79	70.48±0.78	71.12±0.59	68.15±0.82	70.25±0.98	<u>71.35±0.60</u>	<b>71.49±1.85</b>
	40	67.39±1.46	65.60±0.98	68.57±0.51	68.65±0.67	66.64±1.14	68.56±1.10	<u>69.39±0.82</u>	<b>69.45±0.89</b>
	50	67.53±0.76	66.20±0.57	69.06±0.32	67.88±1.37	67.24±1.31	69.83±0.80	<u>70.26±0.95</u>	<b>70.65±0.66</b>
PUR	10	78.60±4.90	79.40±3.87	84.90±1.51	84.10±4.15	74.70±3.03	85.20±2.41	<u>85.70±2.07</u>	<b>86.20±2.51</b>
	20	61.90±1.82	60.80±1.67	<u>67.15±1.65</u>	63.10±2.58	59.35±1.64	67.10±4.10	66.80±2.95	<b>67.75±0.50</b>
	30	54.13±3.00	52.53±1.32	57.70±1.50	<b>59.23±1.53</b>	54.53±1.74	57.53±1.27	<u>59.17±1.10</u>	58.93±2.03
	40	50.92±2.41	49.00±2.07	53.27±1.44	52.47±1.54	49.70±1.23	53.02±1.30	<u>53.75±2.16</u>	<b>54.78±1.60</b>
	50	48.50±1.57	47.60±0.83	52.32±0.61	50.22±2.23	48.86±1.68	52.66±1.32	<b>53.86±1.54</b>	<u>53.44±1.64</u>

Table 5: Performance metrics comparisons on Face95 database between K-means, NMF, GNMF, HNMF, NTR-MU, GNTR-MU, HGNTR-MU and LraHGNTR-MU methods. We divide the database into different subset. Each subset contains  $k_{Face95}$  categories.

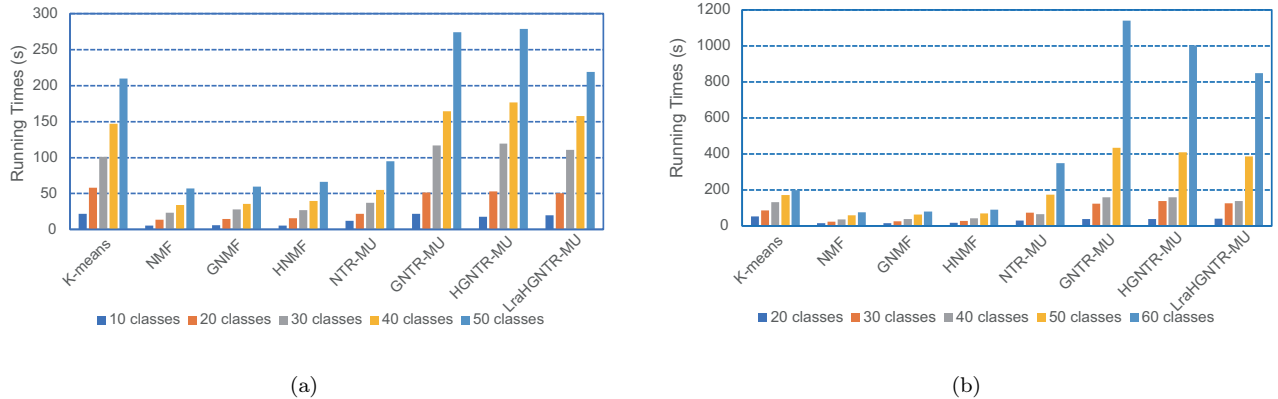


Figure 5: The running time of various algorithms subset in different number of categories. (a) ORL. (b) GT.

- Low-rank approximation methods can eliminate the noise effectively. The reason is that in most datasets with noise, noise usually does not have the low rank property, so replacing the original tensor  $\mathcal{X}$  with an approximate tensor  $\tilde{\mathcal{X}}$  can ignore the noise and thus avoid the influence of noise.

	$k_{Face96}$	K-means	NMF	GNMF	HNMF	NTR-MU	GNTR-MU	HGNTR-MU	lraHGNTR-MU
ACC	20	76.80±6.96	77.00±3.82	77.65±5.70	79.05±2.04	66.35±3.89	75.90±4.13	<u>80.05±4.73</u>	<b>81.00±6.14</b>
	30	74.40±2.48	<u>76.83±2.69</u>	72.76±3.87	72.70±3.93	71.63±2.45	71.66±2.72	76.67±4.79	<b>78.87±3.87</b>
	40	69.85±4.97	<b>74.60±2.35</b>	66.97±3.66	69.17±4.10	66.27±2.21	71.57±2.71	72.25±2.24	<u>72.47±4.03</u>
	50	68.46±1.46	68.76±1.33	69.02±3.10	71.38±2.49	66.64±1.98	71.32±4.15	<u>74.20±3.00</u>	<b>74.32±2.06</b>
	60	67.50±2.42	70.06±2.06	70.78±2.78	69.56±1.45	64.76±3.37	71.95±3.03	<u>72.43±4.10</u>	<b>72.50±2.35</b>
	NMI	20	85.55±2.77	85.85±1.56	89.25±1.97	89.96±0.70	78.44±2.90	88.37±1.74	<b>89.98±2.52</b>
30		86.75±1.73	88.23±1.11	88.81±1.47	89.58±1.80	85.57±1.88	89.87±1.06	<b>91.20±1.10</b>	<u>91.08±1.31</u>
40		86.77±1.40	88.02±0.56	87.52±0.52	88.05±1.50	84.37±0.95	89.37±0.57	<b>89.57±0.81</b>	<u>89.55±0.85</u>
50		86.52±1.01	87.20±0.40	88.04±0.95	88.10±1.08	85.08±0.72	89.62±1.08	<b>90.37±0.85</b>	<u>89.96±0.53</u>
60		86.88±1.03	88.57±0.47	88.55±0.81	88.29±0.70	85.10±1.87	90.29±0.83	<u>90.86±0.52</u>	<b>91.02±0.43</b>
PUR		20	79.60±5.19	80.80±2.60	82.50±4.34	83.40±1.77	70.30±4.00	81.20±2.55	83.10±4.28
	30	77.73±2.03	80.36±1.76	78.36±2.83	78.70±3.18	75.10±1.73	77.83±1.92	81.30±3.47	<b>82.93±2.36</b>
	40	74.55±3.39	78.57±1.38	73.32±2.32	75.32±3.02	70.35±1.73	77.20±1.79	<u>77.50±2.03</u>	76.75±2.60
	50	72.70±1.23	73.48±1.01	74.26±2.15	76.04±1.81	69.98±1.94	76.78±3.18	<b>78.48±2.41</b>	<u>78.34±1.54</u>
	60	72.15±1.86	75.13±1.35	75.30±1.89	74.41±0.62	68.81±2.96	76.65±2.40	<b>77.73±2.02</b>	<u>77.00±0.82</u>

Table 6: Performance metrics comparisons on Face96 database between K-means, NMF, GNMF, HNMF, NTR-MU, GNTR-MU, HGNTR-MU and LraHGNTR-MU methods. We divide the database into different subset. Each subset contains  $k_{Face96}$  categories.

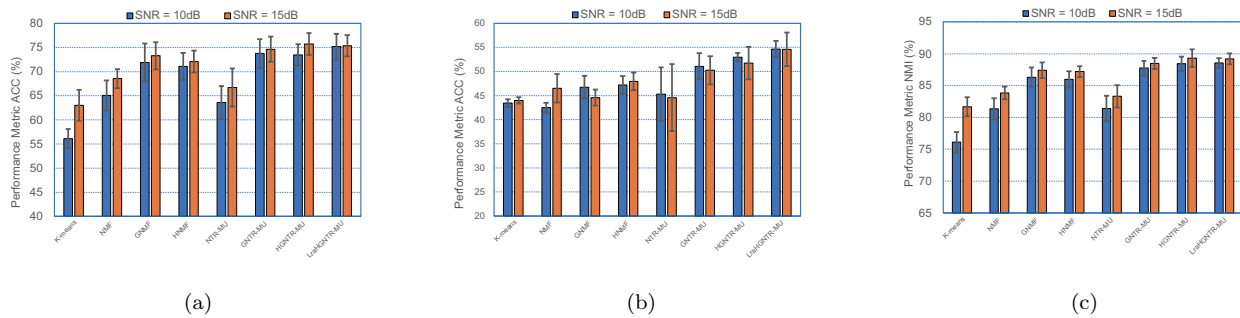
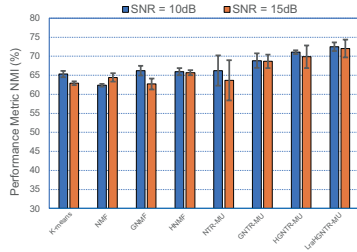


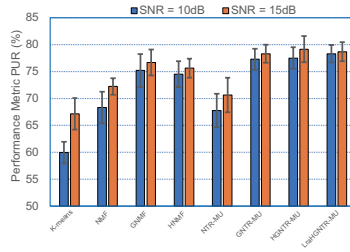
Figure 6: Performance metrics (%) comparisons on between K-means, NMF, GNMF, HNMF, NTR-MU, GNTR-MU, HGNTR-MU and LraHGNTR-MU methods for noise-added ORL and GT database. (a) ACC on ORL. (b) ACC on GT. (c) NMI on ORL.

#### 4.6. Parameter Sensitivity

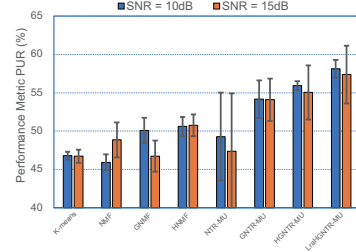
In order to investigate the effect for our model on the situation of parameter changing, we need to carry out parameter sensitivity test. Considering that our algorithms has three parameters that can be adjusted, which are the number of inner iterations  $t$ , the number of nearest neighbours  $k$  and the graph regularization parameter  $\beta$ , we use the method of controlling variables. We divide the experiment into three cases: (1) fix  $k = 5$  and  $\beta = 0.1$ , and choose  $t \in \{20, 40, 60, 80\}$ ; (2) fix  $t = 20$  and  $\beta = 0.1$ , and choose  $k$  to vary from 3 to 6; (3) fix  $t = 20$  and  $k = 5$ , and choose  $\beta \in \{0.1, 0.2, 0.3, 0.4, 0.5, 0.6\}$ .



(a)

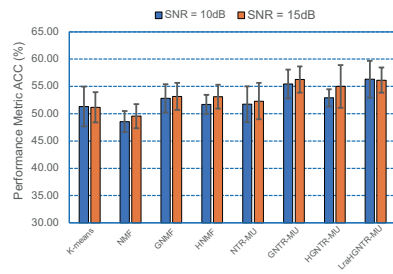


(b)

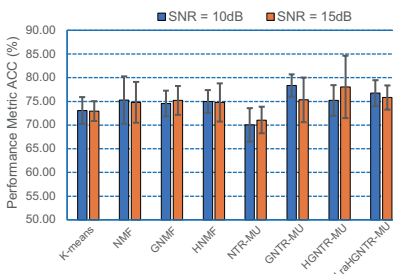


(c)

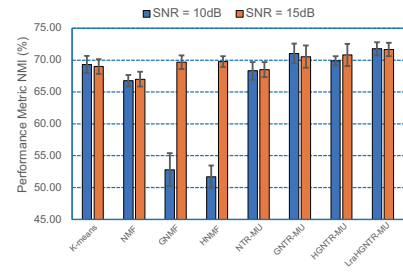
Figure 7: Performance metrics (%) comparisons on between K-means, NMF, GNMF, HNMF, NTR-MU, GNTR-MU, HGNTNTR-MU and LraHGNTNTR-MU methods for noisy-added ORL and GT database. (a) ACC on GT. (b) ACC on ORL. (c) PUR on GT.



(a)

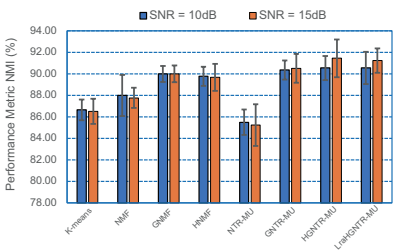


(b)

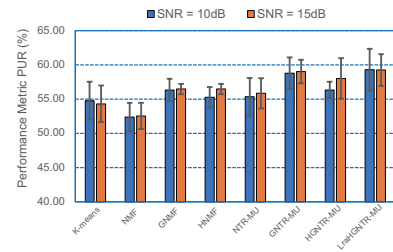


(c)

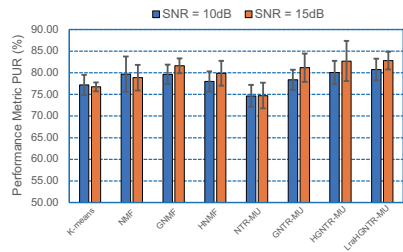
Figure 8: Performance metrics (%) comparisons on between K-means, NMF, GNMF, HNMF, NTR-MU, GNTR-MU, HGNTNTR-MU and LraHGNTNTR-MU methods for noisy-added ORL and GT database. (a) NMI on Face95. (b) PUR on Face96. (c) PUR on Face95.



(a)



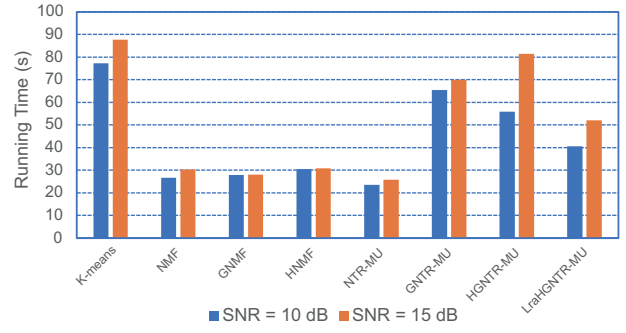
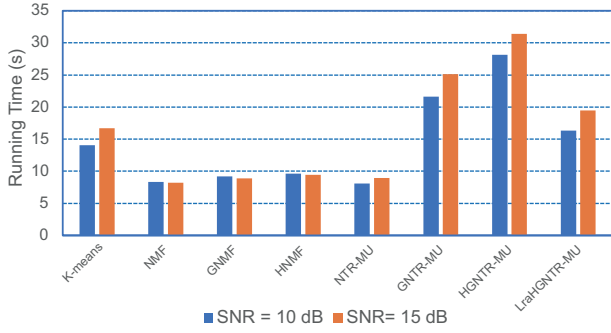
(b)



(c)

Figure 9: Performance metrics (%) comparisons on between K-means, NMF, GNMF, HNMF, NTR-MU, GNTR-MU, HGNTNTR-MU and LraHGNTNTR-MU methods for noisy-added ORL and GT database. (a) NMI on Face96. (b) PUR on Face95. (c) PUR on Face96.

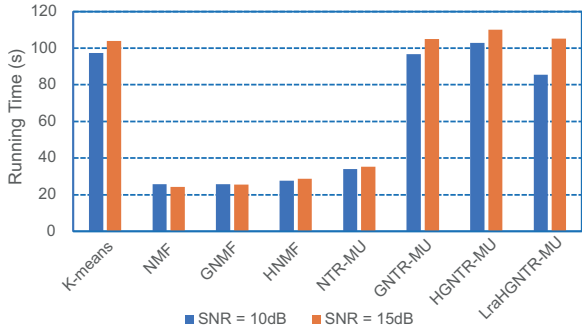
*Fig.12* and *Fig.13* present the clustering performance of the HGNTNTR and LraHGNTNTR across different parameters on the two public databases. It can be observed that the performances of HGNTNTR and LraHGNTNTR algorithms across different parameters are quite stable. The ACC, NMI, and PUR change little when the number of inner iterations  $t$  rises from 20 to 80, so  $t$  can be selected around 20 to balance the calculation cost and fitting error. It can be observed that the ACC, NMI, and PUR are stable when  $k$  in the range of 3 – 6. It can be noted that the hypergraph regularization parameter  $\beta$  also has a relatively weak effect on the performance of our both algorithms.



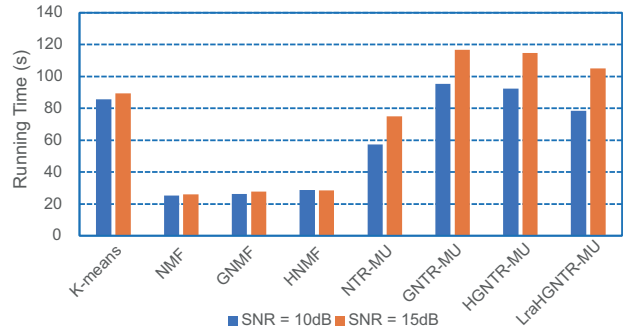
(a)

(b)

Figure 10: Running time comparisons on between K-means, NMF, GNMF, HNMF, NTR-MU, GNTR-MU, HGNTNTR-MU and LraHGNTNTR-MU methods for noise-added ORL and GT database. (a) ORL. (b) GT.



(a)



(b)

Figure 11: Running time comparisons on between K-means, NMF, GNMF, HNMF, NTR-MU, GNTR-MU, HGNTNTR-MU and LraHGNTNTR-MU methods for noise-added Face95 and Face96 database. (a) Face95. (b) Face96.

#### 4.7. Convergence Analysis

We construct a tensor  $\mathcal{X} \in \mathbb{R}^{40 \times 40 \times 40 \times 40}$  by random selection obeying uniform distribution between 0 and 1, and add independent Gaussian noisy with SNR = 10 dB and SNR = 15 dB on this tensor. Then we decomposition it by HGNTNTR and LraHGNTNTR. We count the convergence evolution of the error respectively in *Fig.14*.

Our algorithms can reach a stable value after one hundred iterations. It can be proved that both algorithms are convergent. Particularly, we can see the LraHGNTNTR has a faster convergence rate in the first half part of the iteration process. It can verify that the convergence of the low-rank approximate method is faster. And our low-rank approximation method always reaches the stable convergence value firstly. Regretfully, in the condition of noisy-added tensor data, when the convergence is about to complete, our convergence accuracy of LraHGNTNTR is a little weaker than the HGNTNTR, there is a slight difference, this may is related to the heavy Gaussian noise added on the certain synthetic manual tensor data, it has completely random properties in the statistic. And *fig.15* shows the relative performance in terms of running time and final fitting error. A similar conclusion has been shown in

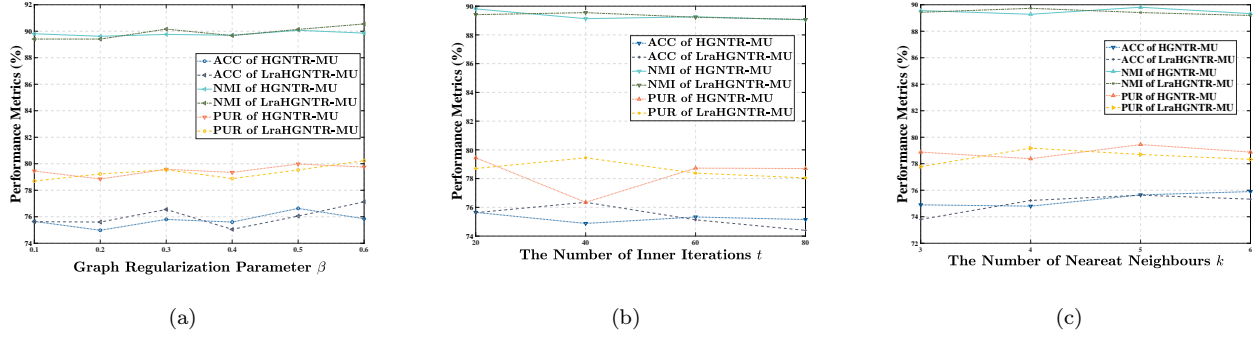


Figure 12: The algorithm performance curve on ORL database in different parameters. (a) The graph regularization parameter  $\beta$ . (b) The number of inner iterations  $t$ . (c) The the number of nearest neighbours  $k$ .

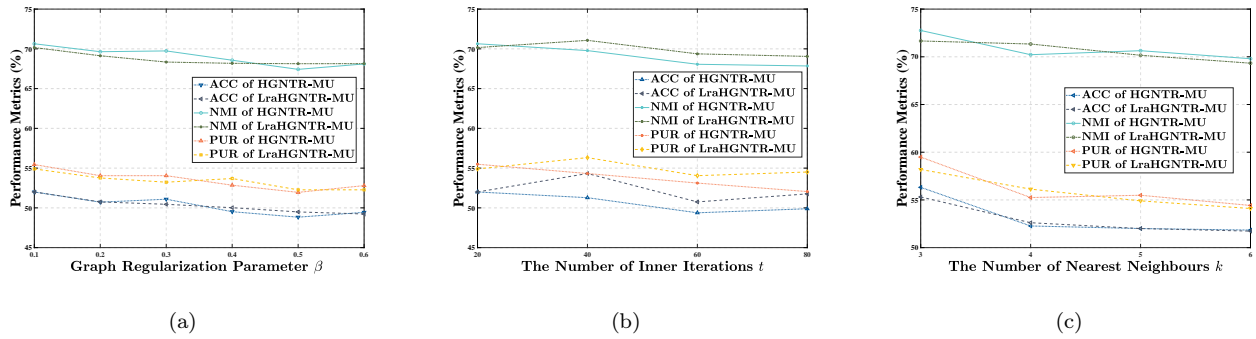


Figure 13: The algorithm performance curve on GT database in different parameters. (a) The graph regularization parameter  $\beta$ . (b) The number of inner iterations  $t$ . (c) The number of nearest neighbours  $k$ .

[16].

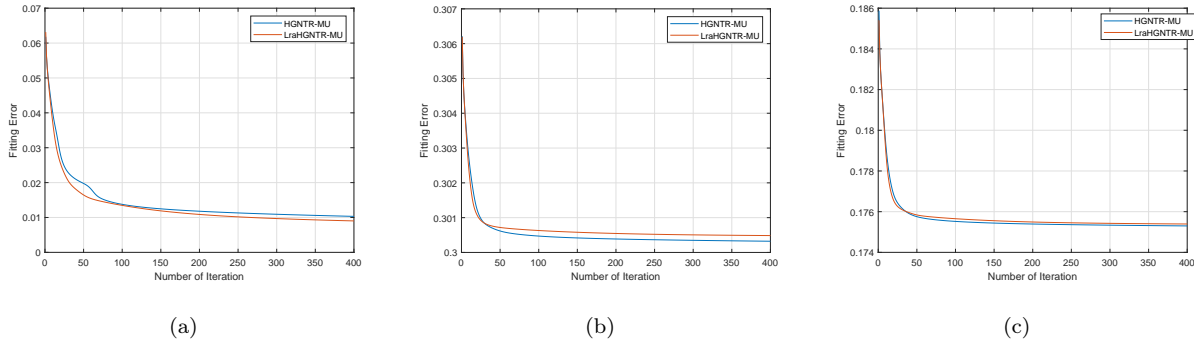


Figure 14: The convergence curve on tensor  $\mathcal{X}$  and noisy-added  $\mathcal{X}$ . The horizontal axis is the number of iterations. The vertical axis is the fitting error. (a) Original tensor. (b) Noisy-added tensor with SNR = 10 dB. (c) Noisy-added tensor with SNR = 15 dB.

#### 4.8. Basis Visualization

In order to compare the ability that extracts the parts-based features from database objects by each algorithm, we visual the basis matrices that are extracted from the ORL and GT database in *Fig.16* and *Fig.17*. For the

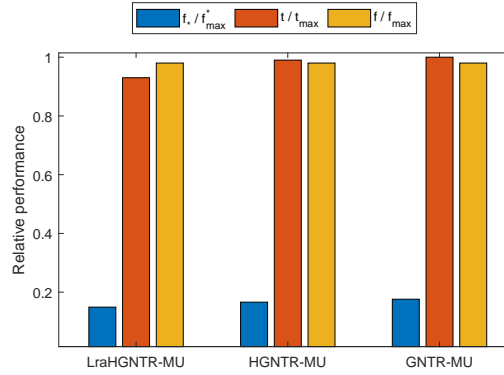


Figure 15: The comparison of performance in terms of runtime and the final fitting accuracy on different algorithms.  $f^*$  and  $f_{max}^*$  denote the noiseless fitting error and max noiseless fitting error.  $t$  and  $t_{max}$  denote the each running time and max running time among them.  $f$  and  $f_{max}$  denote the noisy-added fitting error and max noise-added fitting error.

high-dimensional databases, such as ORL and GT, the matrix methods show very limited capabilities, so that they produce ghost faces, while the tensor methods can produce the more sparse representation. The nonnegativity of the tensor decomposition produces about two main advantages: (1) it can represent the certain potential structure of the data and be physically interpretable. (2) it can reduce the dimensionality of the data and memory storage costs. By comparing all methods, our algorithms HGNTN and LraHGNTN have a higher degree of sparsity. And at the same time, they retain more physically meaningful features.

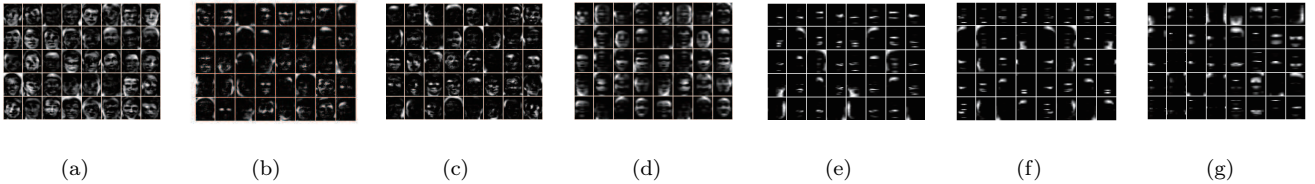


Figure 16: Visual images of base-matrix based on different algorithms for ORL database. (a) NMF. (b) GNMF. (c) HNMF. (d) NTR-MU. (e) GNTN-MU. (f) HGNTN-MU. (g) LraHGNTN-MU.

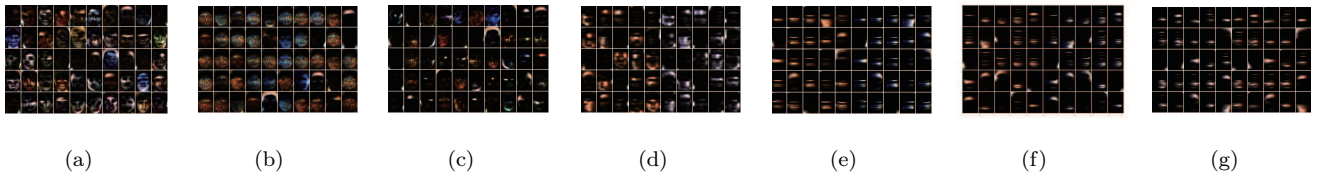


Figure 17: Visual images of base-matrix based on different algorithms for GT database. (a) NMF. (b) GNMF. (c) HNMF. (d) NTR-MU. (e) GNTN-MU. (f) HGNTN-MU. (g) LraHGNTN-MU.



## 5. Conclusion

In this paper, we propose the method of HGNTNTR. Each dimension information of the third-order tensor is expressed as the corresponding three-order core tensor. At the same time, compared with ordinary manifold graph learning, hypergraph manifold learning can explore more high-order manifold structure information. An efficient optimization method based on multiplicative updating rules (MUR) is developed. Considering the computational complexity of the algorithm, we use the low-rank approximation method to reduce the running time. The proposed HGNTNTR and LraHGNTNTR can achieve better performance than state-of-the-art (SOTA) algorithms.

## 6. Acknowledgement

The authors would like to thank...

## References

- [1] D. D. Lee, H. S. Seung, Learning the parts of objects by non-negative matrix factorization, *Nature* 401 (6755) (1999) 788–791.
- [2] A. Cichocki, D. Mandic, L. De Lathauwer, G. Zhou, Q. Zhao, C. Caiafa, H. A. Phan, Tensor decompositions for signal processing applications: From two-way to multiway component analysis, *IEEE signal processing magazine* 32 (2) (2015) 145–163.
- [3] Q. Zhao, M. Sugiyama, L. Yuan, A. Cichocki, Learning efficient tensor representations with ring-structured networks, in: *ICASSP 2019-2019 IEEE International Conference on Acoustics, Speech and Signal Processing (ICASSP)*, IEEE, 2019, pp. 8608–8612.
- [4] L. Yuan, C. Li, D. Mandic, J. Cao, Q. Zhao, Tensor ring decomposition with rank minimization on latent space: An efficient approach for tensor completion, in: *Proceedings of the AAAI Conference on Artificial Intelligence*, Vol. 33, 2019, pp. 9151–9158.
- [5] Y. Yu, G. Zhou, N. Zheng, S. Xie, Q. Zhao, Graph regularized nonnegative tensor ring decomposition for multiway representation learning, *arXiv preprint arXiv:2010.05657* (2020).
- [6] M. Belkin, P. Niyogi, V. Sindhwani, Manifold regularization: A geometric framework for learning from labeled and unlabeled examples., *Journal of machine learning research* 7 (11) (2006).
- [7] M. Belkin, P. Niyogi, Laplacian eigenmaps and spectral techniques for embedding and clustering., in: *Nips*, Vol. 14, 2001, pp. 585–591.
- [8] D. Cai, X. He, J. Han, T. S. Huang, Graph regularized nonnegative matrix factorization for data representation, *IEEE transactions on pattern analysis and machine intelligence* 33 (8) (2010) 1548–1560.

- [9] J. Yu, D. Tao, M. Wang, Adaptive hypergraph learning and its application in image classification, *IEEE Transactions on Image Processing* 21 (7) (2012) 3262–3272.
- [10] A. Bretto, Hypergraph theory, An introduction. Mathematical Engineering. Cham: Springer (2013).
- [11] D. Zhou, J. Huang, B. Schölkopf, Learning with hypergraphs: Clustering, classification, and embedding, *Advances in neural information processing systems* 19 (2006) 1601–1608.
- [12] K. Zeng, J. Yu, C. Li, J. You, T. Jin, Image clustering by hyper-graph regularized non-negative matrix factorization, *Neurocomputing* 138 (2014) 209–217.
- [13] W. Yin, Z. Ma, Q. Liu, Hyperntf: A hypergraph regularized nonnegative tensor factorization for dimensionality reduction, *arXiv preprint arXiv:2101.06827* (2021).
- [14] J. B. Tenenbaum, V. De Silva, J. C. Langford, A global geometric framework for nonlinear dimensionality reduction, *science* 290 (5500) (2000) 2319–2323.
- [15] P.-G. Martinsson, V. Rokhlin, M. Tygert, A randomized algorithm for the decomposition of matrices, *Applied and Computational Harmonic Analysis* 30 (1) (2011) 47–68.
- [16] G. Zhou, A. Cichocki, S. Xie, Fast nonnegative matrix/tensor factorization based on low-rank approximation, *IEEE Transactions on Signal Processing* 60 (6) (2012) 2928–2940.
- [17] G. Zhou, A. Cichocki, Q. Zhao, S. Xie, Efficient nonnegative tucker decompositions: Algorithms and uniqueness, *IEEE Transactions on Image Processing* 24 (12) (2015) 4990–5003.
- [18] T. G. Kolda, B. W. Bader, Tensor decompositions and applications, *SIAM review* 51 (3) (2009) 455–500.
- [19] Q. Zhao, G. Zhou, S. Xie, L. Zhang, A. Cichocki, Tensor ring decomposition, *arXiv preprint arXiv:1606.05535* (2016).
- [20] Y. Chen, W. He, N. Yokoya, T.-Z. Huang, X.-L. Zhao, Nonlocal tensor-ring decomposition for hyperspectral image denoising, *IEEE Transactions on Geoscience and Remote Sensing* 58 (2) (2019) 1348–1362.
- [21] Y.-D. Kim, S. Choi, Nonnegative tucker decomposition, in: *2007 IEEE Conference on Computer Vision and Pattern Recognition*, IEEE, 2007, pp. 1–8.
- [22] T. Hazan, S. Polak, A. Shashua, Sparse image coding using a 3d non-negative tensor factorization, in: *Tenth IEEE International Conference on Computer Vision (ICCV’05) Volume 1*, Vol. 1, IEEE, 2005, pp. 50–57.
- [23] W. Wang, V. Aggarwal, S. Aeron, Efficient low rank tensor ring completion, in: *Proceedings of the IEEE International Conference on Computer Vision*, 2017, pp. 5697–5705.
- [24] L. Yuan, C. Li, J. Cao, Q. Zhao, Randomized tensor ring decomposition and its application to large-scale data reconstruction, in: *ICASSP 2019-2019 IEEE International Conference on Acoustics, Speech and Signal Processing (ICASSP)*, IEEE, 2019, pp. 2127–2131.

- [25] J. A. Bengua, P. N. Ho, H. D. Tuan, M. N. Do, Matrix product state for higher-order tensor compression and classification, *IEEE Transactions on Signal Processing* 65 (15) (2017) 4019–4030.
- [26] Y. Pan, J. Xu, M. Wang, J. Ye, F. Wang, K. Bai, Z. Xu, Compressing recurrent neural networks with tensor ring for action recognition, in: *Proceedings of the AAAI Conference on Artificial Intelligence*, Vol. 33, 2019, pp. 4683–4690.
- [27] I. V. Oseledets, Tensor-train decomposition, *SIAM Journal on Scientific Computing* 33 (5) (2011) 2295–2317.
- [28] C. Hong, J. Yu, J. Li, X. Chen, Multi-view hypergraph learning by patch alignment framework, *Neurocomputing* 118 (2013) 79–86.
- [29] C. Wang, J. Yu, D. Tao, High-level attributes modeling for indoor scenes classification, *Neurocomputing* 121 (2013) 337–343.
- [30] S. Agarwal, K. Branson, S. Belongie, Higher order learning with graphs, in: *Proceedings of the 23rd international conference on Machine learning*, 2006, pp. 17–24.
- [31] Y. Huang, Q. Liu, F. Lv, Y. Gong, D. N. Metaxas, Unsupervised image categorization by hypergraph partition, *IEEE Transactions on Pattern Analysis and Machine Intelligence* 33 (6) (2011) 1266–1273.
- [32] Z. Tian, T. Hwang, R. Kuang, A hypergraph-based learning algorithm for classifying gene expression and arraycgh data with prior knowledge, *Bioinformatics* 25 (21) (2009) 2831–2838.
- [33] Y. Huang, Q. Liu, S. Zhang, D. N. Metaxas, Image retrieval via probabilistic hypergraph ranking, in: *2010 IEEE computer society conference on computer vision and pattern recognition*, IEEE, 2010, pp. 3376–3383.
- [34] S. Huang, H. Wang, Y. Ge, L. Huangfu, X. Zhang, D. Yang, Improved hypergraph regularized nonnegative matrix factorization with sparse representation, *Pattern Recognition Letters* 102 (2018) 8–14.
- [35] P. Drineas, R. Kannan, M. W. Mahoney, Fast monte carlo algorithms for matrices ii: Computing a low-rank approximation to a matrix, *SIAM Journal on computing* 36 (1) (2006) 158–183.
- [36] N. Halko, P.-G. Martinsson, J. A. Tropp, Finding structure with randomness: Probabilistic algorithms for constructing approximate matrix decompositions, *SIAM review* 53 (2) (2011) 217–288.
- [37] M. W. Mahoney, Randomized algorithms for matrices and data, *arXiv preprint arXiv:1104.5557* (2011).
- [38] C. F. Caiafa, A. Cichocki, Generalizing the column–row matrix decomposition to multi-way arrays, *Linear Algebra and its Applications* 433 (3) (2010) 557–573.
- [39] N. Vannieuwenhoven, R. Vandebril, K. Meerbergen, On the truncated multilinear singular value decomposition, *Numerical Analysis and Applied Mathematics Section* (2011).

- [40] A. Huang, et al., Similarity measures for text document clustering, in: Proceedings of the sixth new zealand computer science research student conference (NZCSRSC2008), Christchurch, New Zealand, Vol. 4, 2008, pp. 9-56.